Delayed four-wave-mixing spectroscopy in molecular crystals: A nonperturbative approach

D. P. Weitekamp, Koos Duppen, and Douwe A. Wiersma
Picosecond Laser and Spectroscopy Laboratory, Department of Chemistry, University of Groningen, Nijenborgh 16, 9747-AG Groningen, The Netherlands
(Received 13 September 1982)

The delayed or time-domain four-wave-mixing experiment is treated in the regime of intense near-resonant pulses. The interaction with the radiation during both pump and probe pulses is considered to all powers of the electric field amplitude. Analytical results are obtained for an effective four-level system. These include the dependence of the coherence amplitudes on the ratio of the pump-field intensities when there is a large vibrational discrepancy between ground and excited electronic states and a general solution for the unitary time development during the probe pulse. For the first time, delayed coherent anti-Stokes Raman scattering is detected from highly dilute (10-ppm) guest molecules. Illustrative examples are presented for the system of pentacene in benzoic acid at low temperature. Vibronic-free induction decay and the effect of field inhomogeneity across the beam profile are found to be essential for understanding the observed intensity and spectral distribution of the signal beam in the region of optimum pulse intensity.

I. INTRODUCTION

A. Background

The class of coherent nonlinear optical phenomena known as resonance-enhanced four wave mixing has proven to be a versatile tool for the spectroscopic dissection of the multilevel systems characteristic of molecular electronic, vibrational, and rotational degrees of freedom. By far the greatest number of studies have been performed in the regime of weak fields and steady-state response which is described by the third-order nonlinear susceptibility $\chi^{(3)}$ Refs. 1–7. This tensor quantity describes the induced material polarization at a certain observation frequency which is proportional to a third power of one, two, or three applied frequencies. For the case of interest here the polarization is at $\omega_3=(2\omega_1-\omega_2)$ in response to applied fields at ω_1 and ω_2. It is given by

$$P^{(3)}=\chi^{(3)}(\omega_3,\omega_1,-\omega_2,\omega_1)E^2(\omega_1)E(\omega_2) \qquad (1.1)$$

with

$$\chi^{(3)}=\chi_R^{(3)}+\chi_{NR}^{(3)} . \qquad (1.2)$$

The relationship between this material property and the states of the system is revealed particularly by the positions and widths of resonances in $\chi_R^{(3)}$ as the applied frequencies are varied. A background signal accounted for by $\chi_{NR}^{(3)}$ arises from processes which are nonresonant and thus nearly dispersionless in the experimental range of ω_1, ω_2, and ω_3.

Of particular interest to us here are those cases where $(\omega_1-\omega_2)$ is equal to a vibrational energy

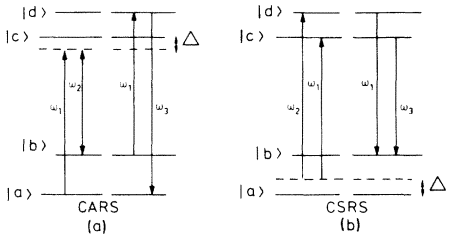

FIG. 1. The relationship between the optical frequencies and the guest molecule energy levels for delayed four wave mixing. Four energy levels are indicated by solid horizontal lines. States $|a\rangle$ and $|b\rangle$ are the ground state and a vibrationally excited state in the S_0 electronic manifold. States $|c\rangle$ and $|d\rangle$ are the corresponding states in the electronically excited S_1 manifold. Initially all population is in state $|a\rangle$. (a) In ground-state CARS, the preparation of coherence between $|a\rangle$ and $|b\rangle$ is achieved by simultaneous pulses at ω_1 and ω_2 where $(\omega_1-\omega_2)=\omega_{ba}$ as indicated by the two arrows on the left. The break in the center indicates the delay t_1. On the right the probe pulse at ω_1 causes emission at $\omega_3\simeq(2\omega_1-\omega_2)$. As drawn, this probe process is exactly resonant at $\omega_1=\omega_{db}$. (b) Analogous relationships are shown for excited-state CSRS. As discussed in Appendix B, the delayed version of excited-state CSRS does not require pure dephasing to be an allowed process in contrast to the steady-state experiment described by $\chi^{(3)}$.

difference in a ground or excited state and ω_1, ω_2, and ω_3 are all resonant or nearly resonant with electronic or vibronic transitions.[8-13] Two possible relationships of the frequencies to the system energy levels are sketched in Fig. 1. The arrangement of Fig. 1(a), where $\omega_1 > \omega_2$, is resonant coherent anti-Stokes Raman scattering (CARS), while that of Fig. 1(b) where $\omega_1 < \omega_2$ is resonant coherent Stokes Raman scattering (CSRS). The frequencies of Fig. 1(a) are chosen for resonance with a ground-state vibration $[(\omega_1-\omega_2)=\omega_{ba})]$ while Fig. 1(b) shows resonance with an excited-state vibration $[(\omega_2-\omega_1)=\omega_{dc}]$. Other arrangements are possible. Recent applications have succeeded in resolving individual vibrational resonances in both ground and excited states in condensed phases.[10,12,13]

A quite different approach to studying vibrational transitions at $\omega_1-\omega_2$ is the method of delayed or time-domain four wave mixing. In these experiments the system is first prepared in a state of vibrational coherence. This may be accomplished for intense Raman modes in concentrated systems by stimulated scattering of a single picosecond pulse.[14-17] A more general approach, and the one taken here, is excitation by simultaneous pulses at ω_1 and ω_2.[18-31] After a variable delay t_1, a probe pulse at ω_1 is scattered off the material excitation giving rise to emission at ω_3. This pulse sequence is depicted in Fig. 2. Again the energy diagrams of Fig. 1 are relevant, but now there is an actual time ordering as suggested by the break in the energy levels which separates preparation and probing processes.

Experimental studies with the sequence of Fig. 2 have been made on vibrations in concentrated organic liquids,[19,21,27] both vibrations[24,26] and librons[25] in pure molecular crystals, and on vibrational bands in the gas phase.[23]

Previous theoretical analyses of the time-domain experiment of Fig. 2 have been made by using perturbation expansions in the field amplitudes. For example, the preparation process during the first two pulses has been treated by invoking an effective Hamiltonian quadratic in the electric field which acts on the two-level vibrational system[16,27] [$|a\rangle$ and $|b\rangle$ in Fig. 1(a)]. In another approach, second-order time-dependent perturbation theory was used on a system with an arbitrary number of intermediate levels [$|c\rangle$ and $|d\rangle$ of Fig. 1(a)] to obtain an expression for the prepared coherence between states $|a\rangle$ and $|b\rangle$ which is quadratic in the fields.[22] The probe process (coherent Raman scattering) has been treated as linear in the probe pulse field amplitude.[16,22] A similar perturbative approach is taken in a very recent work which catalogs those transient four-wave-mixing processes which occur with three pulses up to third order in the fields.[28]

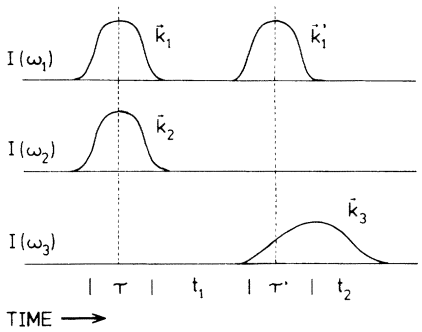

FIG. 2. Pulse sequence for delayed four wave mixing. Experiment begins with the simultaneous arrival at the sample of two pulses at frequencies ω_1 and ω_2 traveling in the directions $\vec{k}_1$ and $\vec{k}_2$ and persisting for a time τ. After a variable delay t_1 a probe pulse follows of length τ', frequency ω_1, and direction $\vec{k}'_1$. Pulse widths in τ and τ' are typically 6 psec (FWHM). Signal consists of the coherent emission near the frequency $\omega_3=(2\omega_1-\omega_2)$ in the direction $\vec{k}_3=\vec{k}_1+\vec{k}'_1-\vec{k}_2$ which occurs both during and after the probe pulse. Pulse sequence is repeated every 100 msec.

In the steady-state or continuous-wave CARS and CSRS experiments it is essential to work at low input powers in order that the frequency dependence of the signal, in fact, reveal, through the $\chi^{(3)}$ formalism, the energy differences and relaxation processes of the field-free system. Several groups have commented on the broadening of line shapes seen as the laser power is increased.[5,9,13,32] In practice, the power at ω_1 and ω_2 is reduced until no further lineshape changes are observed. Theoretical predictions of saturation effects in CARS have recently been made for various regimes of pulse intensities and relaxation times using either higher-order perturbation theory[5] or by considering a system of three levels and calculating steady states[33,34] and slowly decaying transients.[33] A recent discussion of CARS saturation effects covers the two-level limit on various time scales.[35]

B. Motivation

In the delayed experiment the use of intense saturating fields is not only permissible, but highly desirable. The information on the transverse relaxation of the prepared coherence comes not from the frequency dependence of the signal, but from the decay as a function of the delay t_1 during which no perturbing fields are applied. Thus power broadening is not a concern. Rather, a principle experimental concern is the optimization of the pulse parameters with respect to the signal intensity.

There are other reasons for using high power. In a system with nearly degenerate vibrations it allows one to simultaneously excite coherence between several pairs of levels and observe beats as well as decay as t_1 is incremented. In a system with a continuous distribution of vibrational frequencies it would be desirable to eliminate the inhomogeneity by an echo pulse at $t_1/2$ which would reverse the sign of a component of the vibrational coherence and cause rephasing at t_1 limited only by the transverse relaxation time.[36–40] Finally, there are coherences whose relaxation times do not appear in $\chi^{(3)}$ in the absence of pure dephasing.[4,12,41–43] An example is the observation of excited-state vibrational dephasing with the CSRS arrangement of Fig. 1(b). As we will see, the use of short pulses in a delayed CSRS experiment will make this an allowed process at any temperature.

In all of these cases perturbative treatments of the dynamics during the pulses offer little or no guidance as to the feasibility of the experiment or optimization of the experimental parameters. The steady-state $\chi^{(3)}$ formalism is entirely inappropriate since the pulses in time-domain are nearly always comparable to, or shorter than, the relaxation times being measured; a steady-state situation is not reached. Perturbative treatment of transients leaves open the question of how to determine and describe the region of optimal pulse intensity where one would like to perform the experiments.

C. Outline

The approach taken here is to treat the interaction with the fields nonperturbatively. In order to do so it is necessary to limit the Hilbert space to some finite and tractable set of states. It is furthermore desirable to work in an interaction representation in which temporal and spatial dependence of the applied fields due to pulse propagation is removed. Hamiltonians for such an approach are derived in Sec. II for a four-level model.

In Sec. III A a general form for the dependence of the four-wave-mixing signal on the pulse parameters is derived. This formulation poses a number of dynamical problems to be solved. In Sec. III B the preparation process depicted on the left-hand side of Fig. 1(a) is treated for the case of a large vibrational discrepancy between ground and excited states. The probe process is simpler and is treated analytically for an arbitrary vibrational discrepancy in Sec. III C. Section IV demonstrates the applicability of delayed CARS to the molecular mixed crystal system of dilute pentacene in benzoic acid. Low-temperature vibrational dephasing times are measured and power broadening and saturation effects are demonstrated. The saturation of the probe process on resonance is considered in detail and shown to depend on an interplay of free induction decay (FID) and field inhomogeneity effects. Section V indicates some additional applications for the nonperturbative approach and summarizes.

II. EFFECTIVE HAMILTONIANS

A. The internal Hamiltonian

The Hamiltonian for the system in the absence of applied fields is implicit in the energy-level diagram of Fig. 1. The origin of these levels and their description in terms of the electronic and nuclear coordinates will be of no consequence for the calculations, but will appear only through spectroscopic parameters. It will be assumed, however, that no additional states are significantly populated on the time scale of the experiment. One type of system where this will frequently be a good approximation is that of the dilute guest in a mixed molecular crystal. The other vibrational states can be neglected because in the frequency range of interest the signal is dominated by resonant processes which leave these nonresonant states unperturbed. Intersystem crossing to a triplet state is assumed to remove a negligible fraction of the molecules from the singlet manifold on the subnanosecond time scale of the pulse sequence of Fig. 2. The repetition rate of the sequence will be kept low enough so that the initial condition is always that of equilibrium. The coupling of the four-level system to the lattice will be described, where necessary, by phenomenological relaxation rates. The understanding of these rates in terms of phonon scattering processes is one application for the experiments analyzed here.

With these considerations the system Hamiltonian can be written in bracket notation and frequency units (rad/sec) as

$$\mathscr{H}_0=\omega_a|a\rangle\langle a|+\omega_b|b\rangle\langle b|+\omega_c|c\rangle \times\langle c|+\omega_d|d\rangle\langle d| \ . \tag{2.1}$$

It is convenient to rearrange the terms to obtain a form which eliminates one parameter:

$$\mathscr{H}_0=\omega_A A_z+\omega_X X_z+(J/2)(2A_zX_z) \ . \tag{2.2}$$

A term proportional to the identity operator has been dropped in going from (2.1) to (2.2). This has no effect on the dynamics and amounts to choosing a zero average energy. The remaining orthogonal, diagonal, traceless operators may be related to the number operators of (2.1) and to pseudospin operators[44,45] by

$$A_z=\tfrac{1}{2}(|a\rangle\langle a|+|b\rangle\langle b|-|c\rangle\langle c|-|d\rangle\langle d|)$$
$$=(I_z^{ac}+I_z^{bd})=(I_z^{ad}+I_z^{bc}), \quad (2.3a)$$
$$X_z=\tfrac{1}{2}(|a\rangle\langle a|-|b\rangle\langle b|+|c\rangle\langle c|-|d\rangle\langle d|)$$
$$=(I_z^{ab}+I_z^{cd})=(I_z^{ad}-I_z^{bc}), \quad (2.3b)$$
$$2A_zX_z=\tfrac{1}{2}(|a\rangle\langle a|-|b\rangle\langle b|-|c\rangle\langle c|+|d\rangle\langle d|)$$
$$=(I_z^{ab}-I_z^{cd})=(I_z^{ac}-I_z^{bd}). \quad (2.3c)$$

The last equality on the right of each of Eqs. (2.3a)–(2.3c) expresses a linear dependence among the population difference operators I_z^{ij}. These operators are defined as

$$I_z^{ij}=\tfrac{1}{2}(|i\rangle\langle i|-|j\rangle\langle j|).$$

The coefficients of (2.2) are related to those of (2.1) by

$$\omega_a=\tfrac{1}{2}[(\omega_a+\omega_b)-(\omega_c+\omega_d)], \quad (2.4a)$$
$$\omega_X=\tfrac{1}{2}[(\omega_a-\omega_b)+(\omega_c-\omega_d)], \quad (2.4b)$$
$$J/2=\tfrac{1}{2}[(\omega_a-\omega_b)-(\omega_c-\omega_d)]. \quad (2.4c)$$

These represent, respectively, an average electronic quantum, an average vibrational quantum, and one-half the vibrational energy discrepancy between ground and excited states.

B. The optical interaction

The Hamiltonian describing the interaction of the system with the optical frequency fields is treated semiclassically and in the dipole approximation. In frequency units this is

$$\mathscr{H}_{\rm opt}(R,\vec{r},t)=\hbar^{-1}\vec{\mu}\cdot\vec{E}(R,\vec{r},t), \quad (2.5)$$

where $\vec{\mu}$ is the dipole moment operator within the four-level system and $\vec{E}(R,\vec{r},t)$ is the applied laser field. This field will be due to three monochromatic (transform limited) beams with different propagation directions:

$$\vec{E}(R,\vec{r},t)=\vec{E}^{(1)}(R,\vec{r},t)+\vec{E}^{(1')}(R,\vec{r},t)+\vec{E}^{(2)}(R,\vec{r},t), \quad (2.6a)$$

where

$$\vec{E}^{(\alpha)}(R,\vec{r},t)=\vec{E}_0^{(\alpha)}(R,t_r)\cos(\vec{k}_\alpha\cdot\vec{r}-\omega_\alpha t+\phi_\alpha). \quad (2.6b)$$

The first two terms of (2.6a) are both at frequency ω_1, but have propagation vectors $\vec{k}_1$ and $\vec{k}_1'$ differing from one another in direction.

The amplitude factors $E_0^{(\alpha)}(R,t_r)$ account for the spatial variation of the field as a function of radial distance R from the beam center and for the relatively slow (picosecond) amplitude modulation as the pulse rises and falls. The time variables appearing in amplitude factors of position-dependent fields or in material system operators will always implicitly be retarded times, e.g., $t_r=\vec{k}_\alpha\cdot\vec{r}/\omega_\alpha$. For the present, the arguments (R,t_r) will be dropped and these factors will be approximated as square waves in both time and space corresponding to the idealization of plane waves which are either on or off. In Sec. IV integration over a more realistic beam cross section will be necessary.

Significant fractional absorption or frequency conversion of the applied fields is neglected, as is any action of the induced fields on the system. These assumptions are valid for sufficiently dilute systems in the absence of host resonances.

With these considerations, the interaction (2.5) may be expanded in the eigenbasis of $\mathscr{H}_0$ as

$$\mathscr{H}_{\rm opt}(\vec{r},t)=\hbar^{-1}\sum_{\alpha=1,1',2}\sum_{i,j}\langle i|\vec{\mu}\cdot\vec{E}_0^{(\alpha)}|j\rangle\times\cos(\vec{k}_\alpha\cdot\vec{r}-\omega_\alpha t+\phi_\alpha)|i\rangle\langle j|. \quad (2.7)$$

Defining Rabi frequencies

$$\epsilon_{ij}^{(\alpha)}=\langle i|\vec{\mu}\cdot\vec{E}_0^{(\alpha)}|j\rangle \quad (2.8a)$$

and assuming

$$\epsilon_{ij}^{(\alpha)}=\epsilon_{ji}^{(\alpha)}, \quad (2.8b)$$

as is the case for linearly polarized fields and states of definite parity, (2.7) can be rewritten in pseudo-spin operators as

$$\mathscr{H}_{\rm opt}(\vec{r},t)=2\sum_{\alpha=1,1',2}\sum_{i<j}\cos(\vec{k}_\alpha\cdot\vec{r}-\omega_\alpha t+\phi_\alpha)\epsilon_{ij}^{(\alpha)}I_x^{ij} \quad (2.9a)$$
$$=2\sum_{\alpha=1,1',2}\sum_{i<j}[\cos(\vec{k}_\alpha\cdot\vec{r}+\phi_\alpha)\cos\omega_\alpha t+\sin(\vec{k}_\alpha\cdot\vec{r}+\phi_\alpha)\sin\omega_\alpha t]\epsilon_{ij}^{(\alpha)}I_x^{ij}. \quad (2.9b)$$

Only off-diagonal operators,

$$I_x^{ij}=\tfrac{1}{2}(|i\rangle\langle j|+|j\rangle\langle i|), \quad (2.10a)$$

$$I_y^{ij}=\frac{-i}{2}(|i\rangle\langle j|-|j\rangle\langle i|), \quad (2.10b)$$

are kept in (2.9), again consistent with states of definite parity.

C. The generalized rotating frame

In order to remove the rapid time dependence of $\mathscr{H}_{\rm opt}(\vec{r},t)$ at the optical frequencies, a generalized rotating-frame interaction representation can be entered through an operator

$$T=\exp(i\mathscr{T}t)\ , \tag{2.11}$$

where $\mathscr{T}$ is a general diagonal operator

$$\mathscr{T}=\alpha A_z+\beta X_z+\gamma(2A_zX_z) \tag{2.12}$$

defined by some parameters α, β, and γ whose choice will depend on the specific case. The Hamiltonian in this time-dependent frame is found by transforming (2.2) and (2.9) and adding the acceleration correction:

$$\mathscr{H}^T(\vec{r},t)=T\mathscr{H}_0T^\dagger+T\mathscr{H}_{\rm opt}(\vec{r},t)T^\dagger+i\dot{T}T^\dagger \tag{2.13a}$$

$$=(\mathscr{H}_0-\mathscr{T})+T\mathscr{H}_{\rm opt}(\vec{r},t)T^\dagger \tag{2.13b}$$

$$=\mathscr{H}_0^T+\mathscr{H}_{\rm opt}^T(\vec{r},t)\ . \tag{2.13c}$$

In order to calculate the term $\mathscr{H}_{\rm opt}^T(\vec{r},t)$, the action of T on the off-diagonal operators is needed. The commutation relations for the pseudospin operators are as follows[44,45]:

$$[I_p^{ij},I_q^{ij}]=iI_r^{ij} \tag{2.14a}$$

($p,q,r=x,y,z$ or cyclic permutation)

$$[I_x^{ij},I_y^{ik}]=\frac{-i}{2}I_x^{jk}\ , \tag{2.14b}$$

$$[I_{x,y}^{ij},I_{x,y}^{ik}]=\frac{i}{2}I_y^{jk}\ , \tag{2.14c}$$

$$[I_x^{ij},I_z^{ik}]=\frac{i}{2}I_y^{ij}\ , \tag{2.14d}$$

$$[I_y^{ij},I_z^{ik}]=\frac{i}{2}I_x^{ij}\ , \tag{2.14e}$$

$$[I_z^{ij},I_z^{ik}]=0\ , \tag{2.14f}$$

$$[I_p^{ij},I_q^{kl}]=0\ . \tag{2.14g}$$

The rotating-frame time-dependent operators needed in $\mathscr{H}_{\rm opt}^T(\vec{r},t)$ are found from (2.14a) and (2.14c) to be

$$TI_x^{ac}T^\dagger=I_x^{ac}\cos[(\alpha+\gamma)T]-I_y^{ac}\sin[(\alpha+\gamma)t]\ , \tag{2.15a}$$

$$TI_x^{bd}T^\dagger=I_x^{bd}\cos[(\alpha-\gamma)t]-I_y^{bd}\sin[(\alpha-\gamma)t]\ , \tag{2.15b}$$

$$TI_x^{ab}T^\dagger=I_x^{ab}\cos[(\beta+\gamma)t]-I_y^{ab}\sin[(\beta+\gamma)t]\ , \tag{2.15c}$$

$$TI_x^{cd}T^\dagger=I_x^{cd}\cos[(\beta-\gamma)t]-I_y^{cd}\sin[(\beta-\gamma)t]\ , \tag{2.15d}$$

$$TI_x^{ad}T^\dagger=I_x^{ad}\cos[(\alpha+\beta)t-I_y^{ad}\sin[(\alpha+\beta)t]\ , \tag{2.15e}$$

$$TI_x^{bc}T^\dagger=I_x^{bc}\cos[(\alpha-\beta)t]-I_y^{bc}\sin[(\alpha-\beta)t]\ . \tag{2.15f}$$

Similar expressions hold for the I_y^{ij} operators with x and y subscripts exchanged and the sign of the angle reversed. For example,

$$TI_y^{ac}T^\dagger=I_y^{ac}\cos[(\alpha+\gamma)t]+I_x^{ac}\sin[(\alpha+\gamma)t]\ . \tag{2.16}$$

Substitution of the operators $TI_x^{ij}T^\dagger$ for the operators I_x^{ij} in (2.9) gives the explicit form for $\mathscr{H}_{\rm opt}^T(\vec{r},t)$.

D. Coherent averaging theory

The reason for transforming to a rotating frame is to obtain a time-independent approximation to $\mathscr{H}^T(\vec{r},t)$, which can be used to calculate the dynamics during the pulses to all orders in the field. This effective Hamiltonian is given by coherent averaging theory[46] as

$$\mathscr{H}^T(\vec{r})=\mathscr{H}^{(0)}(\vec{r})+\mathscr{H}^{(1)}(\vec{r})+\cdots\ , \tag{2.17}$$

where

$$\mathscr{H}^{(0)}(\vec{r})=(1/t_c)\int_0^{t_c}\mathscr{H}^T(\vec{r},t)dt\ , \tag{2.18}$$

$$\mathscr{H}^{(1)}(\vec{r})=(-i/2t_c)\int_0^{t_c}\int_0^{t'}[\mathscr{H}^T(\vec{r},t),\mathscr{H}^T(\vec{r},t')]dt'dt\ . \tag{2.19}$$

The lowest-order term or average Hamiltonian is found by substituting (2.13) into (2.18):

$$\mathscr{H}^{(0)}(\vec{r})=\mathscr{H}_0^T+(1/t_c)\int_0^{t_c}\mathscr{H}_{\rm opt}^T(\vec{r},t)dt \tag{2.20a}$$

$$\equiv\mathscr{H}_0^T+\mathscr{H}_{\rm opt}^{T(0)}(\vec{r})\ . \tag{2.20b}$$

The average Hamiltonian $\mathscr{H}^{(0)}$ will account for the resonant and near-resonant interactions while $\mathscr{H}^{(1)}$ gives a first approximation to the power-dependent optical Stark (Bloch-Siegert[47]) effects. The range of usefulness of the expansion (2.17) is largely limited to those cases where $||\mathscr{H}^{(n+1)}||\ll||\mathscr{H}^{(n)}||$. Whether such rapid convergence holds depends on the choice of T and the resulting cycle time t_c and will become clear only when $\mathscr{H}^{(1)}$ is calculated.

E. Specific rotating frames and average Hamiltonians

1. General considerations for specifying T

The parameters α, β, and γ which define T can now be specified by requiring that there be nonvanishing contributions from $\mathscr{H}^T_{\rm opt}(\vec{r},t)$ for processes that are near resonance. This occurs when the frequencies of (2.9) match the rotating-frame modulation frequencies of the individual transition operators which appear as the arguments in (2.15). A further requirement is that at exact resonance between one of the applied frequencies and a system energy difference, the diagonal term $\mathscr{H}^T_0 \equiv (\mathscr{H}_0 - \mathscr{T})$ of (2.13) have identical matrix elements for the states so connected; that is, there is a level crossing in the interaction representation. This latter requirement specifies the direction (sign) of the rotations which define T.

2. Resonance-enhanced ground-state CARS

a. Eliminating the time dependence at ω_1 and ω_2. For the frequencies in the neighborhood of those in Fig. 1(a), these conditions give

$$(\alpha+\gamma) = -\omega_1 \,, \tag{2.21a}$$

$$(\alpha-\beta) = -\omega_2 \,. \tag{2.21b}$$

This is a set of only two equations for the three parameters specifying the generalized rotating frame. A third equation

$$(\beta-\gamma) = -\kappa \tag{2.22}$$

is introduced for convenience, leaving κ unspecified for now.

The difference between the frequencies will be tuned to the ground-state vibration

$$(\omega_1-\omega_2) = \omega_{ba} = -(\omega_x + J/2) \tag{2.23}$$

while the individual frequencies ω_1 and ω_2 may be detuned from exact electronic resonance by an amount Δ such that

$$\omega_1 = \omega_{ca} - \Delta = -(\omega_A + J/2) - \Delta \,, \tag{2.24}$$

$$\omega_2 = \omega_{cb} - \Delta = -(\omega_A - \omega_X) - \Delta \,. \tag{2.25}$$

With these substitutions the diagonal term of (2.13) becomes

$$\begin{aligned}\mathscr{H}^T_0 = \tfrac{1}{2}\{ &-\Delta(I_z^{ac}+I_z^{bc}) \\ &+[(\omega_X - J/2)+\kappa-\Delta](I_z^{ad}+I_z^{bd}) \\ &+[(\omega_X - J/2)+\kappa]I_z^{cd}\} \,.\end{aligned} \tag{2.26}$$

b. Large vibrational discrepancy, three-level average Hamiltonian. The form of (2.26) suggests that the specification of the rotating frame be completed by setting

$$\kappa = -(\omega_X - J/2) = \omega_{dc} \,. \tag{2.27}$$

For this choice, the transformation T will be labeled T_3. Doing so and, in addition, using the identity

$$I_z^{ad}+I_z^{bd} = \tfrac{2}{3}(I_z^{ad}+I_z^{bd}+I_z^{cd}) + \tfrac{1}{3}(I_z^{ac}+I_z^{bc}) \,, \tag{2.28}$$

transforms (2.26) to the form

$$\begin{aligned}\mathscr{H}^{T_3}_0 = &-(2\Delta/3)(I_z^{ac}+I_z^{bc}) \\ &-(\Delta/3)(I_z^{ad}+I_z^{bd}+I_z^{cd}) \,.\end{aligned} \tag{2.29}$$

Note that none of the parameters of (2.2) remain, having all been transformed away.

It is still necessary to evaluate the contribution of the optical terms to the average Hamiltonian (2.20). For the preparation period the terms in (2.9b) from beams 1 and 2 are finite. Substituting (2.21), (2.22), and (2.27) into (2.15) completes the specification of $\mathscr{H}^T_{\rm opt}(\vec{r},t)$ in (2.13). Integration over any long t_c in (2.20) gives

$$\begin{aligned}\mathscr{H}^{T_3(0)}_{\rm opt}(\vec{r}) = &\epsilon^{(1)}_{ac}[I_x^{ac}\cos(\vec{k}_1\cdot\vec{r}+\phi_1)+I_y^{ac}\sin(\vec{k}_1\cdot\vec{r}+\phi_1)] \\ &+\epsilon^{(2)}_{bc}[I_x^{bc}\cos(\vec{k}_2\cdot\vec{r}+\phi_2)+I_y^{bc}\sin(\vec{k}_2\cdot\vec{r}+\phi_2)] \,.\end{aligned} \tag{2.30}$$

The spatial dependence can now be removed by the further transformation

$$\begin{aligned}K(\vec{r}) = &\exp[i(\vec{k}_1\cdot\vec{r}+\phi_1)A_Z] \\ &\times\exp\{i[(\vec{k}_1-\vec{k}_2)\cdot\vec{r}+(\phi_1-\phi_2)]X_z\} \,.\end{aligned} \tag{2.31}$$

The desired average Hamiltonian, independent of the trivial time and space dependence due to pulse propagation is

$$\begin{aligned}\mathscr{H}^{(0)}_3 &= K(\vec{r})[\mathscr{H}^{T_3}_0 + \mathscr{H}^{T_3}_{\rm opt}(\vec{r})]K^{-1}(\vec{r}) \\ &= (2\Delta/3)(I_z^{ac}+I_z^{bc}) + \epsilon^{(1)}_{ac}I_x^{ac} + \epsilon^{(2)}_{bc}I_x^{bc} \\ &\quad -(\Delta/3)(I_z^{ad}+I_z^{bd}+I_z^{cd}) \,.\end{aligned} \tag{2.32}$$

Note that $|d\rangle$ is an eigenstate of (2.32) and that the

last term in parentheses commutes with all operators in the subspace spanned by $|a\rangle$, $|b\rangle$, and $|c\rangle$. This term does not affect the dynamics which is entirely within the lower three states of Fig. 1(a); thus, the subscript 3.

In order to rely on (2.32) for a calculation of the system dynamics during the preparation pulse it is necessary to first establish the conditions under which the higher-order correction terms of (2.17) can safely be neglected. The largest correction will come from $\mathscr{H}_3^{(1)}(\vec{r})$ (2.19) for those terms where the integrand is of constant sign. There are no cross terms between terms of $\mathscr{H}_0^T$ even though they are stationary, since they all commute with one another.

From the area of integration in (2.19) cross terms between $\mathscr{H}_0^{T_3}$ and $\mathscr{H}_{\rm opt}^{T_3}(\vec{r})$ will be no larger than

$$||\mathscr{H}_{3,0,\rm opt}^{(1)}|| < t_c \Delta\epsilon_{ij}^{(\alpha)} \tag{2.33}$$

while those between terms of $\mathscr{H}_{\rm opt}^T(\vec{r})$ will be no larger than

$$||\mathscr{H}_{3,\rm opt,opt}^{(1)}|| < t_c \epsilon_{ij}^{(\alpha)} \epsilon_{jk}^{(\beta)} . \tag{2.34}$$

The cycle time t_c is the shortest period for which $T(t_c)=T(0)=1$. Since the generalized rotating frame used here is defined by several (possible incommensurable) frequencies, this condition might never be exactly met. However, for the applications considered here the frequencies are well separated so a physically plausible approximate cycle time is the period of the lowest frequency. For the choice of T determined by (2.21), (2.22), and (2.27) this is $t_c=(2\pi)/(J/2)$. Thus a conservative criterion for the validity of (2.32) is that

$$\Delta, \epsilon_{ij}^{(\alpha)} \ll J/4\pi . \tag{2.35}$$

This means that both the frequency offset of ω_1 and ω_2 from exact resonance and the Rabi frequencies associated with these fields must be kept much less than the vibrational discrepancy between ground and excited states if the dynamics is to remain restricted to levels $|a\rangle$, $|b\rangle$, and $|c\rangle$.

c. Four-level average Hamiltonian. The restriction (2.35) on the optical fields is not always conveniently achieved in practice. The resonance condition $\Delta=0$ may be violated during preparation in order to make the probing process (Sec. III C) more nearly resonant at $\omega_1=\omega_{db}$. The restriction on the Rabi frequencies is also inconvenient since shorter, more intense pulses allow more rapid relaxation processes to be probed. For these reasons a more general average Hamiltonian is needed.

This can be achieved if we are content to transform away only the average electronic energy and the average vibrational energy and account for the vibrational discrepancy explicitly in the rotating-frame Hamiltonian. In terms of the general transformation of (2.11) and (2.12), this means that $\gamma=0$.

Since (2.21) is still necessary to remove the time dependence at ω_1 and ω_2, the necessary transformation is specified by

$$\alpha=-\omega_1 , \tag{2.36a}$$

$$\beta=-\kappa=-(\omega_1-\omega_2)=-\omega_{ba}=(\omega_x+J/2) , \tag{2.36b}$$

$$\gamma=0 . \tag{2.36c}$$

The diagonal terms (2.26) become

$$\mathscr{H}_0^{T_4}=-\tfrac{1}{2}[\Delta(I_z^{ac}+I_z^{bc})+(J+\Delta)(I_z^{ad}+I_z^{bd})+JI_z^{cd}] . \tag{2.37}$$

The off-diagonal terms in $H_4^{(0)}$ analogous to (2.30) become

$$\mathscr{H}_{\rm opt}^{T_4(0)}(\vec{r})=\epsilon_{ac}^{(1)}[I_x^{ac}\cos(\vec{k}_1\cdot\vec{r}+\phi_1)+I_y^{ac}\sin(\vec{k}_1\cdot\vec{r}+\phi_1)]+\epsilon_{bc}^{(2)}[I_x^{bc}\cos(\vec{k}_2\cdot\vec{r}+\phi_2)+I_y^{bc}\sin(\vec{k}_2\cdot\vec{r}+\phi_2)]$$

$$+\epsilon_{bd}^{(1)}[I_x^{bd}\cos(\vec{k}_1\cdot\vec{r}+\phi_1)+I_y^{bd}\sin(\vec{k}_1\cdot\vec{r}+\phi_1)] . \tag{2.38}$$

The spatial dependence is still removed by $K(\vec{r})$ given by (2.31). The result, which is the generalization of (2.32), is

$$\mathscr{H}_4^{(0)}=K(\vec{r})[\mathscr{H}_0^{T_4}+\mathscr{H}_{\rm opt}^{T_4(0)}(\vec{r})]K^{-1}(\vec{r}) \tag{2.39a}$$

$$=(\epsilon_{ac}^{(1)}I_x^{ac}-\Delta I_z^{ac})+[\epsilon_{bd}^{(1)}I_x^{bd}-(\Delta+J)I_z^{bd}]-J/2(I_z^{ab}+I_z^{cd})+\epsilon_{bc}^{(2)}I_x^{bc} . \tag{2.39b}$$

The diagonal terms of (2.39) are those of (2.37), but have been rewritten for later use with the use of the identities of (2.3). The general solution to evolution under (2.39) requires diagonalization of a 4×4 matrix.

The form (2.39) also describes the Hamiltonian for the probing process (Sec. III C) if $\epsilon_{bc}^{(2)}$ is set to zero and both K and the quantities $\epsilon_{ij}^{(1)}$ are primed to indicate probe pulse parameters. K' has the same form as (2.31) except that the preparation pulse

wave vector k_1 is replaced by the probe pulse wave vector k_1'.

III. DYNAMICAL CALCULATIONS

A. Outline of the calculations

In this section the general form is derived of the dependence of the signal on the Hamiltonians of Sec. II. The fundamental quantity needed is the coherent polarization of the system as a function of the time variables of Fig. 2. This is

$$P(\tau,t_1,\tau',t_2)=\mathrm{Tr}[\rho(\tau,t_1,\tau',t_2)\mu] , \tag{3.1}$$

where ρ is the system density operator. In using (3.1) as the only source term, the contribution to the signal of all incoherent spontaneous emission processes is neglected. This is satisfactory since detection will be over a small solid angle in the direction of coherent emission. As sketched in Fig. 2, it will be necessary to evaluate this both during the probe pulse, where τ' is the running variable and t_2 has not yet entered, and after the probe pulse where an FID may occur in the variable t_2.

For concreteness, CARS detection will be assumed. According to (2.8b) only I_x^{ij} operators occur in μ in the laboratory frame. Furthermore, from the energy-level diagram of Fig. 1 only the term in I_x^{ad} is associated with oscillations near $\omega_3=2\omega_1-\omega_2$ for $\omega_1>\omega_2$. As will become clear, the actual frequency of the detected emission may be somewhat different from ω_3 when intense fields are used. The polarization near ω_3 can be written with laboratory-frame operators as

$$P^{\omega_3}(\tau,t_1,\tau',t_2)=\mu_{ad}\mathrm{Tr}[\rho_{\mathrm{lab}}(\tau,t_1,\tau',t_2)I_x^{ad}] , \tag{3.2}$$

where

$$\rho_{\mathrm{lab}}(\tau,t_1,\tau',t_2) =G(\tau,t_1,\tau',t_2)\rho(0)G^{\dagger}(\tau,t_1,\tau',t_2) . \tag{3.3}$$

G is the propagator for the whole pulse sequence. All the dynamical calculations are performed in the interaction representations defined in Sec. II. The propagator in (3.3) will thus take the form

$$G(\tau,t,\tau',t_2) =T^{\dagger}K'^{\dagger}D(t_2)V(\tau')K'K^{\dagger}F(t_1)U(\tau)KT . \tag{3.4}$$

From right to left, the factors on the right of (3.4) serve to enter the rotating frame (T), enter the k_1 translating frame (K), calculate preparation period dynamics [$U(\tau)$], calculate free evolution during the delay [$F(t_1)$], exit the k_1 translating frame ($K^{\dagger}$), enter the k_1' translating frame (K'), calculate probe pulse dynamics [$V(\tau')$], calculate free evolution after the probe pulse [$D(t_2)$], exit the k_1' translating frame ($K'^{\dagger}$) and exit the rotating frame ($T^{\dagger}$). The forms of T, K, and K' have already been given by (2.11), (2.12), (2.36), and (2.31).

The other factors in (3.4) are the propagators

$$U(\tau)=\exp(-i\mathscr{H}^{(0)}\tau) \tag{3.5}$$

with $\mathscr{H}^{(0)}$ given by (2.32) or (2.39);

$$F(t_1)=\exp(-i\mathscr{H}_0^{T_4}t_1) \tag{3.6}$$

and

$$D(t_2)=\exp(-i\mathscr{H}_0^{T_4}t_2) \tag{3.7}$$

with $\mathscr{H}_0^{T_4}$ given by (2.37) or the diagonal terms of (2.39); and

$$V(\tau')=\exp(-i\mathscr{H}_4^{(0)'}\tau') \tag{3.8}$$

with $\mathscr{H}_4^{(0)'}$ given by (2.39) with $\epsilon_{bc}^{(2)}=0$ and primed pulse parameters.

To minimize calculation of irrelevant terms and to simplify the change of reference frames, (3.2) will be rewritten. Substituting $I_x^{ad}=\frac{1}{2}(|a\rangle\langle d| + |d\rangle\langle a|)$ and using the invariance of the trace to cyclic permutation allows the following rearrangement:

$$P^{\omega_3}(\tau,t_1,\tau',t_2) =(\mu_{ad}/2)\mathrm{Tr}\{[F(t_1)\rho(\tau)F^{\dagger}(t_1)] \times[|a\rangle\langle d|(-\tau',-t_2)]\}+\text{c.c.} \tag{3.9}$$

The quantity

$$\rho(\tau)\equiv U(\tau)KT\rho(0)T^{\dagger}K^{\dagger}U^{\dagger}(\tau) \tag{3.10a}$$

becomes simply

$$\rho(\tau)=U(\tau)\rho(0)U^{\dagger}(\tau) \tag{3.10b}$$

if the initial condition is diagonal. This will be called the prepared operator. The detected operator is defined as

$$|a\rangle\langle d|(-\tau',-t_2) =[KK'^{\dagger}V^{\dagger}(\tau')D^{\dagger}(t_2)K'T]a\rangle \times\langle d[T^{\dagger}K'^{\dagger}D(t_2)V(\tau')K'K^{\dagger}] . \tag{3.11}$$

Both (3.10) and (3.11) are in the rotating frame and in the k_1 translating frame.

The prepared operator (3.10) may be expanded in the eigenoperator basis as

$$\rho(\tau)=\sum_{i,j}\rho_{ij}(\tau)|i\rangle\langle j| . \tag{3.12}$$

A similar expansion after a period t_1 of free evolution gives

$$F(t_1)\rho(\tau)F^{\dagger}(t_1) = \sum_{i,j}\rho_{ij}(\tau)\exp(-i\omega_{ij}^{T}t_1) \times \exp(-t_1/T_2^{ij})\,|\,i\rangle\langle j\,|\ . \tag{3.13}$$

The quantities ω_{ij}^{T} are the differences between the eigenvalues of $|\,i\rangle$ and $|\,j\rangle$ for the rotating-frame Hamiltonian $\mathscr{H}_0^{T}$[4] (2.37). An exponential decay time T_2^{ij} has been included for the coherence present during the delay t_1. Relaxation during pulses will be neglected.

Substituting (3.13) into (3.9), the contribution from a single pair of states to the polarization near ω_3 is

$$P_{ij}^{\omega_3}(\tau,t_1,\tau',t_2)=(\mu_{ad}/2)\rho_{ji}(\tau)\exp(-i\omega_{ij}^{T}t_1)\exp(-t_1/T_2^{ij})\mathrm{Tr}\{\,|\,j\rangle\langle i\,|\,[\,|\,a\rangle\langle d\,|\,(-\tau',-t_2)]\}+\text{c.c.} \tag{3.14}$$

The contributions of the free evolution during period t_2 and of the various changes of representation which appear as operators in (3.11) can now be made explicit. For the ground-state vibrational coherence, (3.14) becomes

$$\begin{aligned}P_{ab}^{\omega_3}(\tau,t_1,\tau',t_2) &=(\mu_{ad}/2)\rho_{ba}(\tau)\exp(-t_1/T_2^{ab})\\ &\times\exp\{i[(\vec{k}_1+\vec{k}'_1-\vec{k}_2)\cdot\vec{r}+(\phi_1+\phi'_1-\phi_2)-(2\omega_1-\omega_2)t]\}\exp(-i\omega_{ad}^{T}t_2)\\ &\times\exp(-t_2/T_2^{ad})\mathrm{Tr}[\,|\,b\rangle\langle a\,|\,V^{\dagger}(\tau')\,|\,a\rangle\langle d\,|\,V(\tau')]+\text{c.c.}\end{aligned} \tag{3.15}$$

The quantity $\exp(-i\omega_{ab}^{T}t_1)$ has been dropped, since for the rotating frame used $\omega_{ab}^{T}=0$. This expression clearly displays the propagation direction $\vec{k}_3=(\vec{k}_1+\vec{k}'_1-\vec{k}_2)$ of the desired wave and the dependence of its phase on that of the pulses through the quantity $\phi_3=(\phi_1+\phi'_1-\phi_2)$. During t_2 the remaining trace factor is constant with τ' set equal to the length of the probe pulse. Then (3.15) is the source for a homogeneous FID at $(2\omega_1-\omega_2+\omega_{ad}^{T})$. In Sec. IV inhomogeneous damping will be included. During the probe pulse (3.15) still applies if t_2 is set to zero and τ' is the running variable. The signal is centered at $(2\omega_1-\omega_2)$, but is amplitude modulated by the τ' dependence of the trace. It remains then to calculate this trace and also the coefficient $\rho_{ab}(\tau)$ of the prepared operator. These calculations are the subject of Secs. III B and III C.

In general, there could be other contributions $P_{ij}^{\omega_3}$ with the same propagation direction arising either from other ground-state vibrations, if more states were included, or from the excited-state vibration. In such a case beats could occur in t_1. For the conditions under which $\rho(\tau)$ will be calculated here and also in the experiments of Sec. IV, this situation does not occur and (3.15) is the entire system polarization contributing in the direction $\vec{k}_3$. The nonresonant contribution to the polarization is not included in (3.15), since to the extent that it is free of dispersion it vanishes for delays greater than a few pulse lengths.

B. Preparation of ground-state coherence: large vibrational discrepancy

In this section the coefficient $\rho_{ba}(\tau)$ of the ground-state vibrational coherence which appears in (3.15) will be calculated for the arrangement of ω_1 and ω_2 shown on the left of Fig. 1(a) in the limit of large vibrational discrepancy discussed in Sec. II E 2. The validity of the calculation is restricted by (2.35) and furthermore we will set $\Delta=0$, which makes it analytically simple for arbitrary ratio of the two laser fields.

The Hamiltonian (2.32) then becomes

$$\mathscr{H}_3^{(0)}=\epsilon_{ac}^{(1)}I_x^{ac}+\epsilon_{bc}^{(2)}I_x^{bc} \tag{3.16a}$$

$$=\epsilon(\cos\theta\, I_x^{ac}+\sin\theta\, I_x^{bc})\ , \tag{3.16b}$$

where

$$\theta\equiv\tan^{-1}(\epsilon_{bc}^{(2)}/\epsilon_{ac}^{(1)}) \tag{3.17}$$

and

$$\epsilon\equiv[(\epsilon_{ac}^{(1)})^2+(\epsilon_{bc}^{(2)})^2]^{1/2}\ . \tag{3.18}$$

The evolution of a three-level system under (3.16) (two simultaneous resonant fields) has been treated previously in different contexts,[48–51] but the particular result needed here does not appear to have been explicitly given.

The initial condition at low temperature consists of all population in the ground state. This is the

density operator

$$\rho(0)=|a\rangle\langle a|=\tfrac{1}{2}(A_z+X_z+2A_zX_z)+\tfrac{1}{4}\mathbb{1}\ . \quad (3.19)$$

Since we want to use a different rotating frame (T_3) for preparation than that (T_4) used for the rest of the pulse sequence, (3.10b) becomes

$$\rho(\tau)=T_4T_3^{\dagger}U_3(\tau)\rho(0)U_3^{\dagger}(\tau)T_3T_4^{\dagger}\ , \quad (3.20)$$

where here

$$U_3(\tau)=\exp[-i\epsilon(\cos\theta\, I_x^{ac}+\sin\theta\, I_x^{bc})\tau]\ . \quad (3.21)$$

The preparation dynamics is readily solved by introducing a tilt operator

$$P=\exp(i2\theta I_y^{ab}) \quad (3.22)$$

and explicitly calculating in a tilted frame so that

$$U_3(\tau)\rho(0)U_3^{\dagger}(\tau)=P^{-1}U_3^{P}(\tau)\rho^{P}(0)U_3^{P\dagger}(\tau)P \quad (3.23)$$

with

$$U_3^{P}(\tau)\equiv PU(\tau)P^{-1}=\exp(-i\epsilon I_x^{ac}\tau) \quad (3.24)$$

and

$$\rho^{P}(0)\equiv P\rho(0)P=\tfrac{1}{3}(|a\rangle\langle a|+|b\rangle\langle b|+|c\rangle\langle c|)+\tfrac{1}{2}(\cos\theta+1)I_z^{ac}$$
$$+\tfrac{1}{6}[3\cos(2\theta)-1](I_z^{ab}-I_z^{bc})-\sin(2\theta)I_x^{ab}\ . \quad (3.25)$$

Carrying out the operations indicated in (3.23) gives

$$\begin{aligned}
&U_3(\tau)\rho(0)U_3^{\dagger}(\tau)\\
&\quad=\tfrac{1}{3}(|a\rangle\langle a|+|b\rangle\langle b|+|c\rangle\langle c|)\\
&\qquad+\{\tfrac{1}{12}[1-3\cos(2\theta)]+\tfrac{1}{4}[1+\cos(2\theta)]\cos(\epsilon\tau)\}(I_z^{ac}+I_z^{bc})\\
&\qquad+\{\tfrac{1}{4}[3\cos(2\theta)-1]\cos(2\theta)+\tfrac{1}{4}[1+\cos(2\theta)]\cos(2\theta)\cos(\epsilon\tau)+\sin^2(2\theta)\cos(\epsilon\tau/2)\}I_z^{ab}\\
&\qquad+\{\tfrac{1}{4}[3\cos(2\theta)-1]\sin(2\theta)+\tfrac{1}{4}[1+\cos(2\theta)]\sin(2\theta)\cos(\epsilon\tau)-\sin(2\theta)\cos(2\theta)\cos(\epsilon\tau/2)\}I_x^{ab}\\
&\qquad+\{\tfrac{1}{2}[1+\cos(2\theta)]\cos\theta\sin(\epsilon\tau)+\sin(2\theta)\sin\theta\sin(\epsilon\tau/2)\}I_y^{ac}\\
&\qquad+\{\tfrac{1}{2}[1+\cos(2\theta)]\sin\theta\sin(\epsilon\tau)-\sin(2\theta)\cos\theta\sin(\epsilon\tau/2)\}I_y^{bc}\ .
\end{aligned} \quad (3.26)$$

Finally, the coefficient needed for (3.15) is, for this case,

$$\begin{aligned}
\rho_{ba}(\tau)&=\mathrm{Tr}[|a\rangle\langle b|\rho(\tau)]\\
&=\tfrac{1}{2}\{\tfrac{1}{4}[3\cos(2\theta)-1]\sin(2\theta)+\tfrac{1}{4}[1+\cos(2\theta)]\sin(2\theta)\cos(\epsilon\tau)\\
&\qquad-\sin(2\theta)\cos(2\theta)\cos(\epsilon\tau/2)\}\ .
\end{aligned} \quad (3.27)$$

There are several features of this function worth noting that are not evident in perturbative treatments. The time dependence of the ground-state vibrational coherence during the preparation pulse has Fourier components at 0, ϵ, and $\epsilon/2$. The relative weight of these components depends on the ratio of the two applied fields through the relation $(\epsilon_{ba}^{(2)}/\epsilon_{ac}^{(1)})=\tan\theta$. This ratio is important for the efficiency of the preparation process. For short times $[(\epsilon\tau)^2\ll 1]$, the coherence amplitude is given by

$$\rho_{ba}(\tau)=-(\epsilon^2\tau^2/16)\sin(2\theta) \quad (3.28a)$$

which can be written as

$$\rho_{ba}(\tau)=-(\tau^2/8)\epsilon_{ac}^{(1)}\epsilon_{bc}^{(2)}\ . \quad (3.28b)$$

This shows the correspondence to the perturbative approaches where the prepared coherence depends on the product of the amplitudes of the applied fields at ω_1 and ω_2.

In Fig. 3 the coherence amplitude ρ_{ba} given by (3.27) is plotted for a fixed pulse length τ of 6 psec with three values of $\epsilon_{ac}^{(1)}$. The ratio $\epsilon_{bc}^{(2)}/\epsilon_{ac}^{(1)}$ is varied from 0.1 to 10 from left to right. The solid curve is in the low-power limit where (3.28) applies. The apparent curvature is due to the logarithmic scaling along the horizontal axis. This curve is magnified vertically by a factor of 10 relative to the axis markings and the other curves. The dashed curve is with a 100-fold increase in beam intensity. The dependence on $\epsilon_{bc}^{(2)}$ is nearly linear for $\epsilon_{bc}^{(2)}<\epsilon_{ac}^{(1)}$, but then saturates and declines. Another 25-fold increase in power gives the dotted curve which shows pronounced oscillations as $\epsilon_{bc}^{(2)}$ is varied.

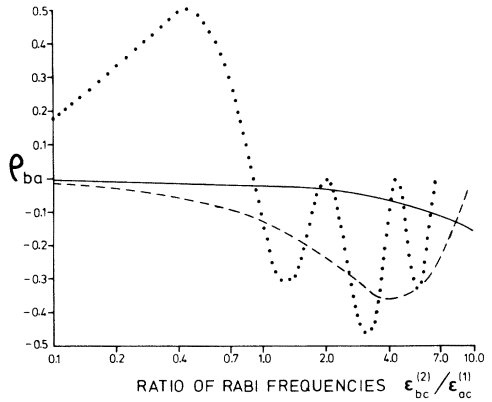

FIG. 3. Dependence of vibrational coherence amplitude on the strength of the preparation pulses. This calculation is done using (3.27) which applies to the case where the preparation pulses are resonant ($\Delta=0$) and the Rabi frequencies $\epsilon_{ac}^{(1)}$ and $\epsilon_{bc}^{(2)}$ are much less than the vibrational discrepancy between ground and excited states. Pulse lengths are fixed at $\tau=6$ psec and three different values of $\epsilon_{ac}^{(1)}$ are chosen. For the lowest value $[(\epsilon_{ac}^{(1)}/2\pi c)=0.1\ \text{cm}^{-1}]$ the prepared coherence amplitude is nearly linear as $(\epsilon_{bc}^{(2)}/2\pi c)$ ranges up to 1 cm^{-1}. This is indicated by the solid curve. Apparent curvature is due to the logarithmic horizontal scale. This curve is scaled up vertically by a factor of 10 relative to the axis markings and the other two curves. Dashed curve is for $(\epsilon_{bc}^{(1)}/2\pi c)=1.0\ \text{cm}^{-1}$. Linearity in $\epsilon_{bc}^{(2)}$ holds approximately for $\epsilon_{bc}^{(2)}<\epsilon_{ac}^{(1)}$, after which the amplitude saturates and declines for larger $\epsilon_{bc}^{(2)}$. Dotted curve is for $(\epsilon_{ac}^{(1)}/2\pi c)=5.0\ \text{cm}^{-1}$. Dependence on $\epsilon_{bc}^{(2)}$ is oscillatory, but the maximum coherence amplitude is achieved.

If an average over $\epsilon\tau$ is taken, then only the first term of (3.27) survives. This average vibrational coherence also changes sign as the ratio of the fields is varied. Here this average is considered simply to indicate the complexities of the dependence on pulse parameters to be expected at high power. Experimentally, averages over pulse angles can arise due to inhomogeneity of the beam across the sample. This type of averaging is considered in Sec. IV and Appendix A.

C. Probe pulse dynamics

1. *General prescription*

For the interaction of the system with the probe pulse, the state $|d\rangle$ is necessarily involved since, as noted in Sec. III A, the CARS signal in the four-level model is a measure of the coherence between levels $|a\rangle$ and $|d\rangle$ arising from coherence initially prepared between $|a\rangle$ and $|b\rangle$. This is expressed by the factor

$$\text{Tr}[\,|b\rangle\langle a|\,V^{\dagger}(\tau')\,|a\rangle\langle d|\,V(\tau')]$$

of Eq. (3.15).

As noted in Sec. III A the relevant Hamiltonian $\mathscr{H}_4^{(0)'}$ is isomorphic with (2.39b) except that $\epsilon_{bc}^{(2)}$ is zero. The remaining terms consist of three mutually commuting operator sums, each of which is collected within a pair of parentheses in (2.39b).

Evolution under these terms can be expressed analytically for any values of the parameters. To this end it is useful to introduce two new tilt transformations:

$$M=\exp(i2\mu I_y^{bd}) \tag{3.29a}$$

with

$$2\mu=\tan^{-1}[(\Delta+J)/\epsilon_{bd}^{(1')}] \tag{3.29b}$$

and

$$N=\exp(i2\eta I_y^{ac}) \tag{3.30a}$$

with

$$2\eta=\tan^{-1}(\Delta/\epsilon_{ac}^{(1')})\ . \tag{3.30b}$$

The Hamiltonian in this doubly tilted frame is

$$\mathscr{H}_{M,N}^{(0)'}=MN\mathscr{H}_4^{(0)'}N^{\dagger}M^{\dagger} \tag{3.31a}$$

$$=-(J/2)X_z+mI_x^{bd}+nI_x^{ac}\ , \tag{3.31b}$$

where

$$m=[(\Delta+J)^2+(\epsilon_{bd}^{(1')})^2]^{1/2} \tag{3.32a}$$

and

$$n=[\Delta^2+(\epsilon_{ac}^{(1')})^2]^{1/2}\ . \tag{3.32b}$$

The diagonal operators in the $J/2$ term have been relabeled as X_Z using the definitions in (2.3b). This is a reminder that alternate forms are available which simplify the calculation

The probe pulse dynamics of any operator I_p^{ij} can now be obtained by a series of rotations defined by single pseudospin operators as follows:

$$\begin{aligned}&I_p^{ij}(-\tau')\\&\quad=V^{\dagger}(\tau')I_p^{ij}V(\tau')\\&\quad=N^{\dagger}M^{\dagger}V_{M,N}^{\dagger}(\tau')(MNI_p^{ij}N^{\dagger}M)V_{M,N}(\tau')MN\end{aligned} \tag{3.33}$$

with

$$\begin{aligned}&V_{M,N}(\tau')\\&\quad=\exp(-i\mathscr{H}_{M,N}^{(0)'}\tau')\\&\quad=\exp[i(J/2)X_Z\tau']\exp(-imI_x^{bd}\tau')\\&\qquad\times\exp(-inI_x^{ac}\tau')\ .\end{aligned} \tag{3.34}$$

2. Probing with $\omega_1=\omega_{db}$

For the experiments of Sec. IV the probe pulse is resonant with ω_{db}. This corresponds to $\Delta=-J$. In this section the general prescription (3.33) will be used to find with these parameters the factor

$$\mathrm{Tr}[\,|\,b\rangle\langle a\,|\,V^\dagger(\tau')\,|\,a\rangle\langle d\,|\,V(\tau')]$$

needed in (3.15).

From (3.29), (3.30), and (3.32) we see that this case corresponds to $\mu=0$, $2\eta=\tan^{-1}(-J/\epsilon_{ac}^{(1')})$, $m=\epsilon_{bd}^{(1')}$, and $n=[J^2+(\epsilon_{ac}^{(1')})^2]^{1/2}$. From (3.33) a straighforward calculation gives

$$\begin{aligned}
&I_x^{ad}(-\tau')\\
&\quad=\cos(\epsilon_{bd}^{(1)}\tau'/2)\{\,I_x^{ad}[\cos(n\tau'/2)\cos(J\tau'/2)-\sin(2\eta)\sin(n\tau'/2)\sin(J\tau'/2)]\\
&\qquad\qquad+I_y^{ad}[\cos(n\tau'/2)\sin(J\tau'/2)-\sin(2\eta)\sin(n\tau'/2)\cos(J\tau'/2)]\\
&\qquad\qquad+I_x^{cd}\cos(2\eta)\sin(n\tau'/2)\sin(J\tau'/2)\\
&\qquad\qquad-I_y^{cd}\cos(2\eta)\sin(n\tau'/2)\cos(J\tau'/2)\}\\
&\qquad+\sin(\epsilon_{bd}^{(1)}\tau'/2)\{\,I_y^{ab}[\cos(n\tau'/2)\cos(J\tau'/2)-\sin(2\eta)\sin(n\tau'/2)\sin(J\tau'/2)]\\
&\qquad\qquad-I_x^{ab}\cos(2\eta)\cos(n\tau'/2)\sin(J\tau'/2)\\
&\qquad\qquad+I_x^{bc}[\sin(n\tau'/2)\cos(J\tau'/2)+\sin(2\eta)\cos(n\tau'/2)\sin(J\tau'/2)]\\
&\qquad\qquad-I_y^{bc}\cos(2\eta)\sin(n\tau'/2)\sin(J\tau'/2)\}\,.
\end{aligned}\tag{3.35}$$

From this expression it is easy to find

$$V^\dagger(\tau')\,|\,a\rangle\langle d\,|\,V(\tau')=I_x^{ad}(-\tau')+iI_y^{ad}(-\tau')\tag{3.36}$$

since

$$I_y^{ad}(-\tau')=V^\dagger(\tau')\exp[-i(\pi/2)X_z]I_x^{ad}\exp[i(\pi/2)X_z]V(\tau')\tag{3.37a}$$

$$=\exp[-i(\pi/2)X_z]I_x^{ad}(-\tau')\exp[i(\pi/2)X_z]\,.\tag{3.37b}$$

The desired trace is

$$\begin{aligned}
&\mathrm{Tr}[\,|\,b\rangle\langle a\,|\,V^\dagger(\tau')\,|\,a\rangle\langle d\,|\,V(\tau')]\\
&\quad=-\sin(\epsilon_{bd}^{(1)}\tau'/2)\{\,[\cos(n\tau'/2)\cos(J\tau'/2)-\sin(2\eta)\sin(n\tau'/2)\sin(J\tau'/2)]\\
&\qquad\qquad+i\cos(2\eta)\cos(n\tau'/2)\sin(J\tau'/2)\}\,.
\end{aligned}\tag{3.38}$$

If (3.38) is broken up into its Fourier components and substituted into (3.15) the result during the probe pulse ($t_2=0$) is

$$\begin{aligned}
&P_{ab}^{\omega_3}(\tau,t_1,\tau')\\
&\quad=(\mu_{ad}/2)\rho_{ba}(\tau)\exp(-t_1/T_2^{ab})\exp[i(\vec{k}_3\cdot\vec{r}+\phi_3)]\\
&\qquad\times\tfrac{1}{8}((\cos2\eta-\sin2\eta-1)\exp\{-i[\omega_3-(n/2)-(J/2)-(\epsilon_{bd}^{(1')}/2)]\tau'\}\\
&\qquad\qquad-(\cos2\eta-\sin2\eta-1)\exp\{-i[\omega_3-(n/2)-(J/2)+(\epsilon_{bd}^{(1')}/2)]\tau'\}\\
&\qquad\qquad-(\cos2\eta-\sin2\eta+1)\exp\{-i[\omega_3-(n/2)+(J/2)-(\epsilon_{bd}^{(1')}/2)]\tau'\}\\
&\qquad\qquad+(\cos2\eta-\sin2\eta+1)\exp\{-i[\omega_3-(n/2)+(J/2)+(\epsilon_{bd}^{(1')}/2)]\tau'\}\\
&\qquad\qquad+(\cos2\eta+\sin2\eta-1)\exp\{-i[\omega_3+(n/2)-(J/2)-(\epsilon_{bd}^{(1')}/2)]\tau'\}\\
&\qquad\qquad-(\cos2\eta+\sin2\eta-1)\exp\{-i[\omega_3+(n/2)-(J/2)+(\epsilon_{bd}^{(1')}/2)]\tau'\}\\
&\qquad\qquad-(\cos2\eta+\sin2\eta+1)\exp\{-i[\omega_3+(n/2)+(J/2)-(\epsilon_{bd}^{(1')}/2)]\tau'\}\\
&\qquad\qquad+(\cos2\eta+\sin2\eta+1)\exp\{-i[\omega_3+(n/2)+(J/2)+(\epsilon_{bd}^{(1')}/2)]\tau'\})+\mathrm{c.c.}
\end{aligned}\tag{3.39}$$

Fourier transformation with respect to the duration of the probe pulse shows that the CARS signal is no longer at ω_3, but is emitted at eight frequencies displaced about ω_3. The hypothetical spectral distribution of the signal which would be obtained in the limit of a long probe pulse is sketched in Fig. 4. The most prominent feature is a shifting of the intensity from ω_3 to $\sim(\omega_3 \pm \epsilon_{bd}^{(1')}/2)$. In the limit of $J \gg \epsilon_{bd}^{(1')}$ this would be the only structure and the probe dynamics would in effect be a two-level problem in which only $|b\rangle$ and $|d\rangle$ are perturbed. The additional structure in Fig. 4 is due to the fact that the transition at ω_{ca} is only off resonance by $\Delta = -J$ and so these states also can be perturbed. As discussed in Sec. IV and Appendix A, the short length of the probe pulse and the inhomogeneity of the Rabi frequencies across the beam profile prevent resolution of the splittings in Fig. 4.

IV. RESULTS AND DISCUSSION

A. Experimental

Single crystals of benzoic acid doped with pentacene (10^{-5} M/M) were mounted in a variable-temperature He cryostat (Oxford Instruments). The light traveled nearly perpendicular to the ab cleavage plane with polarization along the crystal a axis.

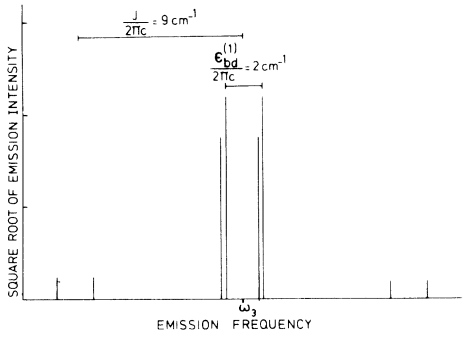

FIG. 4. Fourier analysis of the probe pulse dynamics for $\omega_1 = \omega_{db}$. Spectrum of the emitted light consists of eight lines instead of the single line found in the low-power limit. Illustration is for a Rabi frequency of $(\epsilon_{bd}^{(1)}/2\pi c) = (\epsilon_{ac}^{(1)}/2\pi c) = 2\ \mathrm{cm}^{-1}$ and a discrepancy between ground- and excited-state vibrations of $(J/2\pi c) = -9\ \mathrm{cm}^{-1}$, using (3.39). Dominant feature is a displacement of the intensity from ω_3 to $(\omega_3 \pm \epsilon_{bd}^{(1)}/2)$. This two line approximation would describe the spectrum in the limit that only the levels $|b\rangle$ and $|d\rangle$ were perturbed during probing. Additional structure is due to the involvement of levels $|a\rangle$ and $|c\rangle$. Experimental resolution of this structure would require a long, spatially homogeneous probe pulse.

The experimental arrangement is sketched in Fig. 5 and is similar to that already described for photon echo studies.[52] An acousto-optically mode-locked Ar-ion laser (Spectra Physics, model 171) emits $\sim$100-psec pulses at 514.5 nm with an 80-MHz repetition rate and average power of 760 mW. This output is divided into two beams and used to synchronously pump[53] dye lasers operating at 5884.8 Å (Spectra Physics, model 375 with Rhodamine 6G dye) and 6158.7 Å (Coherent Radiation, model 590 with Rhodamine B dye). These are the frequencies ω_1 and ω_2, respectively. Except where noted, the tuning was achieved with a three plate Lyot filter. The output of each dye laser then consists of $\sim$24 mW in the form of a train of approximately transform limited ($\Delta\nu\Delta t \simeq 0.5$) 6-psec pulses at 80 MHz ($\sim$0.3 nJ/pulse).

Each pulse train passes through two amplifiers consisting of focusing lenses, a dye cell amplifier (Rhodamine 6G at ω_1 and Rhodamine B at ω_2) and a prism and pinhole to discriminate the laser light from dye fluorescence. The amplifiers are pumped by the 532-nm second harmonic of a Nd:YAG laser (Molectron MY 32), which consists of nanosecond pulses at a 10-Hz repetition rate. Glass plates are used to direct a few percent of the YAG output toward each amplifier cell and this is further attenuated so that the final pumping power per pulse is $\sim$80 μJ at the first and $\sim$250 μJ at the second amplifier of each chain. Net amplification is by a factor of $\sim 2\times 10^4$ for the one pulse in 8×10^6 which coincides in the amplifiers with the YAG pulse.

The ω_1 pulses are split into two beams, one of which is sent through a homebuilt variable path length to introduce a relative delay. The ω_2 pulses are sent through an independent variable delay. These three coplanar parallel beams are focused by a single lens such that they converge in the sample with angles of 1°—2° between the wave vectors k_1, k_1', and k_2. Spot size in the sample is $\lesssim 100\ \mu$, as estimated by passing the beams through a pinhole of this size in the same plane as the crystal.

The transmitted beams are again made parallel beyond the sample and the signal beam at $k_3 = k_1 + k_1' - k_2$ is spatially filtered with a pinhole and focused onto the entrance slit of a double monochromator (Spex model 1402). The dispersed signal is measured with a photomultiplier tube (RCA 7265) and processed with a boxcar integrator (EG & G, Model 162 with gated integrator Model 165) to give effective averaging times of a few seconds.

The photodiode (PD) catches a weak reflection of the 80-MHZ argon-ion-laser pulse train. This is divided down to 10 Hz and used to trigger the YAG laser and the boxcar gate.

Pulse lengths were measured using second-

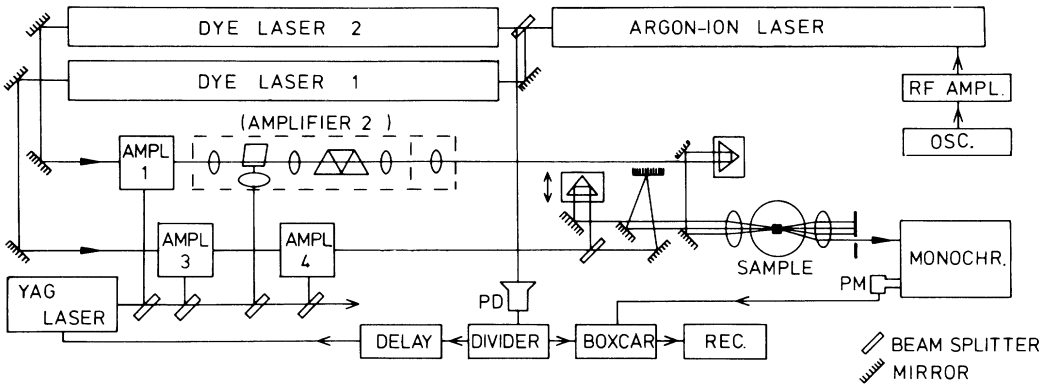

FIG. 5. Experimental arrangement for delayed four wave mixing with psec pulses. An actively mode-locked argon-ion laser synchronously pumps two dye lasers to generate a train of picosecond pulses at ω_1 and at ω_2. A pulse at each frequency is amplified in two stages by dye cells pumped by a YAG laser operating at 10 Hz. Pulse at ω_1 is split into two and one part is sent through a variable path length to introduce a delay. Pulse at ω_2 passes through an independent variable delay. Three pulses enter the sample with wave vectors k_1, k_1', and k_2 and the signal beam exits the sample at $k_3=k_1+k_1'-k_2$. Both spatial filtering and a monochromator are used to eliminate stray laser light. Photomultiplier output is accumulated with a boxcar integrator and plotted on an X-Y recorder as a function of delay time, laser frequency, laser power, or monochromator frequency. YAG laser and boxcar are triggered by the output of the argon-ion laser after division of the trigger signal to 10 Hz.

harmonic generation (SHG) in an ammonium dihydrogen phosphate (ADP) crystal. First, the cavity length of the dye laser is optimized to obtain the shortest pulses by maximizing the ratio of the SHG to the fundamental[54] and then the autocorrelation is measured by varying the delay between pulses.[55] The values reported are $2^{-1/2}$ of the full width at half maximum (FWHM) of the autocorrelation and correspond to the FWHM of the pulse intensity profile, if the pulses are assumed to be Gaussian in time. No difference is found between the autocorrelation functions of amplified and unamplified pulses. In the same way, cross correlation measurements were made between the ω_1 and ω_2 pulses.[56] These indicate some timing jitter between the pulses since they typically have a FWHM of 13 psec for the unamplified pulses and 15 psec for the amplified pulses. The correlation functions for all pulses used fell to less than 1% on either side within 30 psec of the maximum.

Pulse power measurements were made with a pyroelectric joulemeter (Molectron, model J3-05) inserted immediately before the cryostat.

The measurements reported here are CARS experiments performed on the four-level system consisting of the electronic ground state ($|a\rangle$), the vibrationally excited state at 756 cm^{-1} ($|b\rangle$), the zero phonon excited state of S_1 ($|c\rangle$), and the vibrationally excited state of S_1 at 747 cm^{-1} ($|d\rangle$). Details on other vibrations and other hosts will be reported elsewhere.[31] These ground- and excited-state vibrations are prominent features of the fluorescence and absorption spectra, respectively.[10] The inhomogeneous linewidths in our crystals are ~ 1.7 cm^{-1}.

In order to establish that the signals observed arise from the guest pentacene, low-resolution frequency-dependent CARS experiments were performed with long (85-psec) pulses obtained by inserting etalons into the dye lasers. The expected resonance was found at $\omega_1=\omega_{db}$, if ω_1 and ω_2 were varied together with fixed $(\omega_1-\omega_2)$. No CARS signal was observed at $\omega_1=\omega_{ca}$ with resonant $(\omega_1-\omega_2)$, which we tentatively attribute to an optical density effect. The absorption at ω_{ca} was $>95\%$. The time- and power-dependent experiments are thus performed with $\omega_1=\omega_{db}$ and $(\omega_1-\omega_2)=\omega_{ba}$. This corresponds to the arrangement of Fig. 1(a) with $\Delta/2\pi c=9$ cm^{-1}.

B. Transverse vibrational decay

Figure 6 is a typical experimental trace as a function of delay time t_1. The x axis of the chart recorder is synchronized to the stepping motor on the ω_1 delay table. The entire scan takes about 20 minutes. The signal beginning at 125 psec is an independent trace made with the photomultiplier voltage increased to give a tenfold larger signal.

The insert in Fig. 6 shows a logarithmic plot of the decay. The immediate neighborhood of zero delay shows a peaking due both to the greater intensity at ω_1 when preparation and probe beams overlap

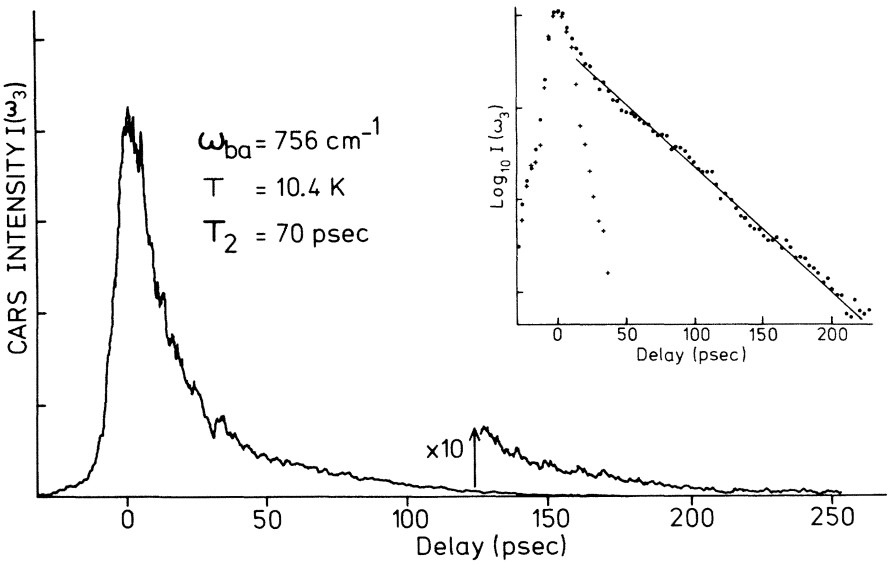

FIG. 6. Decay of the CARS signal with probe pulse delay for the 756-cm^{-1} ground-state vibration of pentacene in benzoic acid at 10.4 K. Horizontal axis is the delay t_1 of Fig. 2. Vertical axis is the boxcar integrator output as this delay is continuously varied and is proportional to signal photon fluence and also to the intensity of the transient $I(\omega_3)$ as sketched in Fig. 2. Initial spike contains contributions from background processes which contribute while preparation and probe pulses overlap. Signal beyond 125 psec is shown amplified by a factor of 10 by increasing the photomultiplier voltage. At probe pulse delay beyond about 20 psec the decay is exponential with a time constant of $T_2/2=35$ psec, as derived from a fit to the logarithmic plot of the data shown as filled circles in the inset at the upper right. Crosses in the inset are for the analogous experiment on the 260-cm^{-1} vibration. This decay was too short for accurate measurement. It serves here to indicate an upper bound on the contribution due to pulse overlap.

and also to nonresonant CARS processes. The relative size of this $t_1=0$ signal to the delayed signal was larger at high pulse power, but this effect was not studied in detail. The delayed signal was measurable and exponential over nearly three orders of magnitude. The slope of the fitted line gives $T_2/2=35\pm1$ psec. This value was constant from 2 to 20 K.

This decay time corresponds to a Lorentzian FWHM of $(\pi c T_2)^{-1}=0.15$ cm^{-1} which is three times narrower than that observed in frequency-dependent CARS[10] and CSRS[13] experiments on the same system. The delayed experiment is insensitive to power broadening and laser linewidth effects, which, in principle, can complicate frequency domain measurements. However, these effects were reported not to be resolution limiting in those studies. We are unable to imagine any mechanism whereby the observed decay could be prolonged relative to the actual decay of the material coherence and thus believe that $T_2=70\pm2$ psec is the low-temperature transverse relaxation time for this $|a\rangle\langle b|$ coherence.

This transverse decay time may be written as the sum of two terms:

$$1/T_2=1/T_2^*+1/2T_1\ , \tag{4.1}$$

where T_1 is the lifetime of the state $|b\rangle$ and T_2^* is a pure dephasing contribution. The present experiment gives no indication of the relative contribution of these terms. This could be determined by a T_1 measurement such as that made by a three-pulse stimulated echo on the 747-cm^{-1} excited-state vibration of pentacene in naphthalene.[57] There it was found that in the low-temperature limit the vibronic $1/T_2$ was equal to $1/2T_1$. It seems likely that this is also the case here.

Another approach to obtain a measure of the pure dephasing is by observing the intensity of a resonance in $\chi^{(3)}$ which vanishes in its absence.[4,12,41–43] This experiment has been performed on the 747-cm^{-1} excited-state CSRS resonance of pentacene in benzoic acid and the pure dephasing due to the local phonon was observed above ~5 K.[12] The signal-to-noise ratio (Fig. 3 of Ref. 12) is not adequate to eliminate the possibility of a $1/T_2^*$ contribution to the $1/T_2$ observed here. Even if $1/T_2^*$ dominated in (4.1), the pure dephasing parameter[12] would be $\Gamma_2\leq0.076$ cm^{-1}. Higher-sensitivity measurements should be possible to rule out such a contribution unequivocally.

In agreement with the frequency domain ground-state CSRS measurements [13] the observed T_2 was essentially independent of temperature up to ~ 20 K, above which a temperature-dependent broadening is evident. This is in contrast to the conclusions of a resonance Raman study of the same vibration in the system of pentacene in naphthalene,[58] where the temperature dependence of the linewidth was fit to the Arrhenius exponential form with an activation energy of ~ 17 cm^{-1} and a low-temperature limit of 0.10 cm^{-1}. This corresponds to a low temperature T_2 of 106 ± 25 psec which is reduced by a factor of ~ 5 at 12 K.

We therefore performed the delayed CARS experiment on pentacene in naphthalene crystals and found that while the low-temperature result of $T_2 = 101\pm 5$ psec is in agreement with the result of Ref. 58, this value had not changed measurably even up to 20 K. In addition, the experiment of Ref. 58 was repeated and confirmed.

This discrepancy leads us to conclude that the temperature-dependent linewidth measured in Ref. 58, in fact, measured *vibronic* dephasing, which is indeed dominated in this temperature range by local phonon activation.[57,59] The delayed CARS experiment measures the actual ground-state vibrational T_2 and this has no measurable contribution from the thermal activation of the local phonon in either host crystal. This is understandable in terms of the de Bree-Wiersma optical Redfield theory[60] if the phonon energy and scattering amplitude are nearly identical in the ground and vibrationally excited states. Then, the fast exchange limit (Ref. 60 and references therein) holds and the contribution to the linewidth which is thermally activated at the local phonon frequency may be undetectably small.

One explanation for the observations of Ref. 58 is that the signal attributed there to near-resonant Raman scattering is actually resonant fluorescence from a distribution of microsites in the wings of the 1.34-cm^{-1}-wide inhomogeneous line. This possibility could be checked by a time-resolved measurement of the right angle luminescence, since only fluorescence would persist for nanoseconds after a pulse of light near the ω_{ca} absorption maximum.

C. Intensity dependence of the dispersed signal

With the delay fixed on the exponential part of the decay, the intensity of the three input beams was varied. Over the available range of power (≤ 2 μJ/pulse) the signal was linear in $I(\omega_2)$. A small degree of saturation was observed as the intensity of the preparation beam at ω_1 was increased. Pronounced saturation effects were observed for the fully resonant probing process and these were studied in detail.

Figure 7 shows the spectrum of the emitted light near $\omega_3 = 2\omega_1 - \omega_2$ (5634.2 Å) for two different probe pulse intensities. The laser frequencies are fixed. Only the monochromator is scanned. Trace *a* is taken with a probe pulse energy of 0.04 μJ. It has a FWHM of 1.2 cm^{-1} and this value was constant when the intensity was lowered further. Trace *b* is with a probe pulse energy of 0.4 μJ and is about four times wider.

In the usual treatments of four wave mixing the production of the light at ω_3 is viewed as a scattering process requiring the simultaneous presence of a material coherence at $(\omega_1 - \omega_2)$ and an applied field at ω_1. In this picture the CARS signal must terminate when the probe pulse does. If this were the case, then the short duration of the probe pulse would set a lower limit on the spectral width of the emitted light. For example, a CARS signal which rose and fell with a Gaussian probe pulse of duration 6 psec would have a FWHM frequency of 2.4

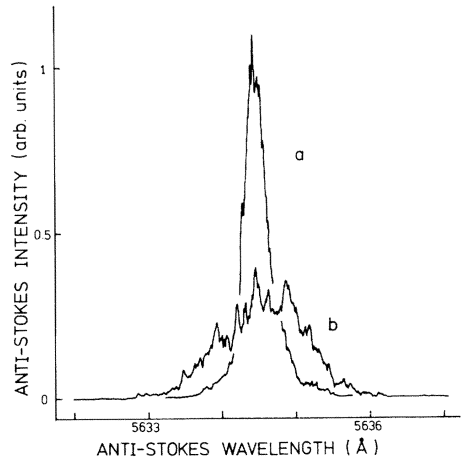

FIG. 7. Spectrally resolved CARS signal centered at $\omega_3 = \omega_{da}$. Vertical axis is the signal fluence at a given monochromator center frequency. Monochromator resolution contributes negligibly to the line shapes. Curve *a* shows the spectral distribution when the probe pulse is weak (0.04 μJ). Spectral width is 1.2 cm^{-1}. This is less than half of the transform limit for a scattering process which follows in time the shape of the probe pulse. This width is explicable only if the signal extends in time beyond the probe pulse in a FID at ω_{da} as predicted by the theory. Curve *b* is taken at high power (0.4 μJ). Spectral width is qualitatively accounted for by the distribution of Rabi frequencies across the beam profile. This distribution eliminates the FID contribution by inhomogeneous optical nutation as confirmed by the simulation of the total fluence measurements in Fig. 8.

cm^{-1}, more than twice that of trace *a*. Similar widths are found for other envelope shapes confined to the duration of the probe pulse. Thus in order to attain the observed spectral width, the CARS emission must extend in a free induction decay beyond the termination of the probe pulse as discussed in connection with (3.15).

An *a priori* estimate for the low-power linewidth can be made by roughly quantifying the form of the time dependence of the signal at ω_3 as sketched in Fig. 2. The signal must rise from zero to some maximum value during the probe pulse and then decay in an inhomogeneous FID after the probe pulse. To simplify, replace the actual probe pulse by a square pulse whose electric field is a least-squares fit to a Gaussian of the same pulse area. This square pulse has a half-width of 5.6 psec and this will be taken as an estimate of the time to half maximum of the signal intensity during the probe pulse. The time scale of the FID after the sudden termination of such a square probe pulse is calculable from the inhomogeneous width of 1.7 cm^{-1} observed in fluorescence. The intensity of the corresponding Gaussian FID would fall to half at $t_2=6.1$ psec. Thus the combined intensity profile is a roughly bell-shaped curve with an intensity half-width in time of 11.7 psec, or in frequency of ~ 1.3 cm^{-1}. This agrees well with the observed value of 1.2 cm^{-1} from trace *a* of Fig. 7. Further evidence for this juxtaposition of scattering and FID will be found when the integrated signal intensity is considered in Sec. IV E.

As indicated by the broad spectrum of trace *b*, the bulk of the signal intensity at high probe pulse power must be occurring in a period of ~ 3 psec indicating that the FID contribution has been suppressed and the emission is occurring during only a fraction of the probe pulse.

D. Probe pulse field inhomogeneity

This power-dependent curtailment of the signal suggests that the coherence is not surviving long enough during the probe pulse to experience the oscillations necessary to give the resolved structure of the theoretical spectrum of Fig. 4. Such a loss of structure is expected if the Rabi frequency is inhomogeneous across the beam profile. In a particular wave front characterized by a constant value of $\vec{k}_1\cdot\vec{r}$, molecules experience an electric field which depends on their distance R from beam center. Since the preparation and probe beams are the same width, the spatial inhomogeneity effects of all the beams are convoluted together.

The model developed here is for the case that the two preparation beam intensities are in the linear-response regime, while the probe beam is treated to all orders. The beams are taken as being coaxial, which is a good approximation at optimum alignment, since they meet at angles of $\lesssim 4°$ and their region of overlap is several times greater than the sample thickness. The distribution for the field intensity of a TEM_{00} beam is taken to be a two-dimensional Gaussian so that the Rabi frequency, which is proportional, has the form

$$\epsilon_{ij}^{(\alpha)}(R)=\epsilon_{ij}^{(\alpha)}(0)\exp(-CR^2)=\epsilon_{ij}^{(\alpha)}u(R)\ , \tag{4.2}$$

where $\epsilon_{ij}^{(\alpha)}(0)$ is the Rabi frequency at beam center and C parameterizes the beam width.

The details of this analysis are in Appendix A. The electric field at the photomultiplier is taken to be proportional to the polarization (3.39) averaged over the distribution (4.2). This spatially averaged field has built into it the possibility of destructive interference between molecules with the same value of $\vec{k}_3\cdot\vec{r}$. This interference occurs when the signal polarization at the beam center change sign relative to that in the surrounding annulus. It amounts to a damping of the coherent scattering, during the probe pulse, which becomes increasingly rapid at higher power.

E. Total signal fluence measurements

The value of the signal intensity at the time when the probe pulse ends becomes the initial value for the subsequent FID. The total signal fluence measured by the slowly responding photomultiplier with the monochromator set to low resolution is the integral over time for these two processes:

$$\Phi_{\rm tot}=\Phi_{\rm pulse}+\Phi_{\rm FID} \tag{4.3a}$$

$$=\int_0^{\tau'} I_{ab}^{\omega_3}(t')dt' + I_{ab}^{\omega_3}(\tau')\int_{\tau'}^{\infty}\exp[-2a^2(t'-\tau')^2]dt'\ . \tag{4.3b}$$

The decay parameter of the Gaussian FID is known from the Gaussian inhomogeneous line shape measured by fluorescence. In terms of the FWHM $\Delta\omega$ (rad/sec),

$$a=\Delta\omega(\ln 2)^{-1/2}/4\ .$$

For the observed value of $\Delta\omega/2\pi c=1.7$ cm^{-1}, the integral in the second term of (4.3b) is 6.5 psec. Thus, as sketched in Fig. 2, the contributions during and after the probe pulse may be comparable.

Figure 8 shows the calculated values of these con-

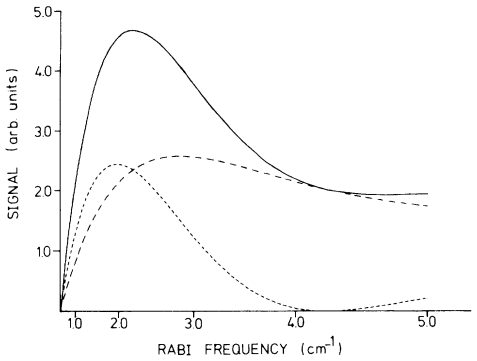

FIG. 8. Simulation of the dependence of the CARS signal on the probe pulse Rabi frequency in the two-level limit. Curve of short dashes is the contribution from the FID after the probe pulse. Its relative size is known from the measured inhomogeneous broadening. Curve of long dashes is the contribution from scattering during the pulse. Calculation uses a square pulse of $\tau'=11.2$ psec, which is a least-squares fit to the electric field profile of a Gaussian pulse with an intensity FWHM of 6 psec. Solid curve is the sum of the two dashed curves and corresponds to the total undispersed signal fluence. Axis markings correspond to $\epsilon_{bd}^{(1')}$ at the center of a Gaussian beam, but the scale is quadratic so as to be proportional to pulse energy. Additional details of the calculation are in Appendix A.

tributions to the signal fluence as a function of probe pulse intensity for the limit $\epsilon_{ac}^{(1)}=0$ or, less stringently, $(\epsilon_{ac}^{(1')})^2/|J| \ll \epsilon_{bd}^{(1')}$. The horizontal axis markings correspond to $\epsilon_{bd}^{(1')}(0)/2\pi c$, the Rabi frequency at beam center, but are plotted quadratically so as to be proportional to pulse intensity. The curve of short dashes is Φ_{FID}. This is proportional to the square of the coherence remaining at the end of the probe pulse. If the beam profile were homogeneous, this curve would be simply $\sin^2(\epsilon_{bd}^{(1')}\tau'/2)$ with fixed τ'. The minimum of the plotted curve corresponds to $(\epsilon_{bd}^{(1')}\tau'/2)=4.4$ rather than π and the second maximum is reduced relative to the first. These deviations are due to the spatial inhomogeneity of the probe pulse.

The curve of long dashes in Fig. 8 is Φ_{pulse}. Without beam inhomogeneity included, this would be proportional to

$$\int_0^{\tau'} \sin^2(\epsilon_{bd}^{(1')}t/2)dt$$

which rises monotonically to $\tau'/2$ at $\epsilon_{bd}^{(1)}/2\pi c=1.5$ cm^{-1} and then oscillates about this value tending toward it asymptotically. The beam inhomogeneity washes out the oscillations and causes a net decline as the peak intensity in successive Rabi cycles is diminished. Thus with an intense inhomogeneous probe pulse, nearly all of the coherent scattering occurs in the initial part of the pulse.

The solid curve is the sum of the dashed curves and represents the observable Φ_{tot}. Note that the upturn at large Rabi frequencies comes from Φ_{FID}.

Figure 9 summarizes the corresponding calculation (Appendix A) for the assumption $\epsilon_{ac}^{(1')}=\epsilon_{bd}^{(1')}$. The nonresonant process, which brings levels $|a\rangle$ and $|c\rangle$ into play, only becomes significant at the higher Rabi frequencies. The curves of short and long dashes in Fig. 9(a) are Φ_{FID} and Φ_{pulse}, respectively. The main difference from Fig. 8 is that now the upturn in Φ_{FID} is moved to $\epsilon_{bd}^{(1')}(0)/2\pi c\simeq 7$ cm^{-1}, which is off the scale of the figure.

Comparison with the experiment is made in Fig. 9(b). The solid curve is Φ_{tot} found by adding the curves of Fig. 9(a) while the dashed curve is the same quantity from Fig. 8. The open circles are the experimental values for Φ_{tot} at the probe pulses ener-

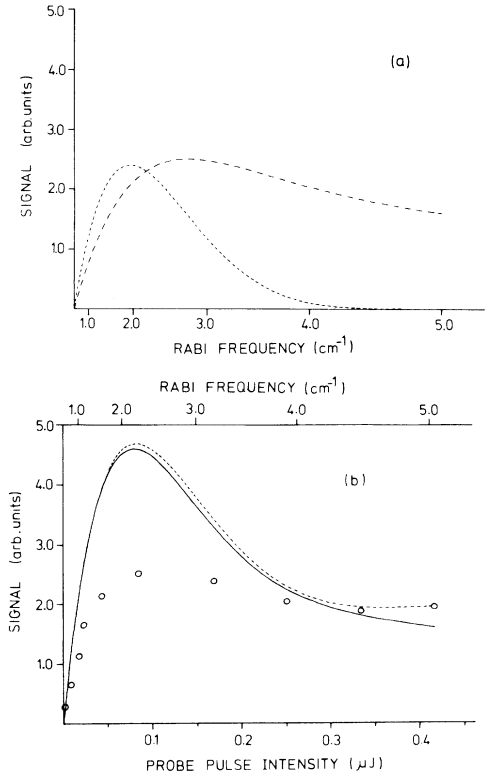

FIG. 9. Dependence of the CARS signal on probe pulse intensity. Calculated curves in (a) are analogous to similar ones of Fig. 8. Difference is that the off-resonant process at ω_{ca} is included with the assumption of equal transition moments $\mu_{ac}=\mu_{bd}$. (b) the solid line is the sum of the dashed lines in (a) while the dashed line is a reproduction of the solid line of Fig. 8. These two calculations of the total undispersed signal are compared to the measured values given by the open circles as a function of probe pulse energy.

gies indicated on the lower horizontal scale.

These were obtained by attenuating the preparation pulses to a fixed value in the linear regime, setting t_1 on the exponential part of the decay, and varying the probe pulse intensity. A correction was made for the bandpass of the double monochromator, which even at its lowest-resolution slit setting attenuated preferentially in the wings. Thus, the reponse of the monochromator was measured and multiplied by the observed line shapes (e.g., Fig. 7) to determine the fractional loss at each intensity.

The data was scaled vertically to match the simulations at the high Rabi frequencies and scaled horizontally to match at the initial maximum. The fit is only qualitative, but establishes that optical nutation of $\epsilon_{bd}^{(1')}\tau' \gtrsim 3\pi$ is attained and shows how the initial and secondary maxima in Φ_{tot} can arise.

The significant overestimate of the initial maximum is presumably due in large part to the neglect of the inhomogeneous line width in the probe pulse dynamics. For molecules in the spectral wings, this leads to less efficient involvement, in fact, than in the calculation, where all molecules are assumed to be resonant with the probe pulse. This neglect is of less importance at the higher intensities, where the Rabi frequencies considerably exceed the inhomogeneous resonance offsets. An additional source for discrepancy between the calculated and observed fluences is that square probe pulses were assumed. These had the same pulse area and were least-squares fits in amplitude to the presumably Gaussian pulses responsible for the measured second-harmonic-generation (SHG) autocorrelations.

An interesting feature of the simulation is that the slight rise in signal fluence at the highest probe intensities seems only to be accounted for by a secondary maximum in Φ_{FID}. Experimentally, this rise is barely within the possible error and it would be desirable to pursue the curve to higher probe pulse energy. Another possibility for establishing the contribution of Φ_{FID} unambiguously would be to move ω_1 slightly away from ω_{db} so that Φ_{pulse} and Φ_{FID} would be at different frequencies ω_3 and ω_{da}, respectively.

V. CONCLUSION

A. Other applications for the nonperturbative approach

The approach taken here to delayed CARS of ground-state vibrations is easily modified to deal with related experiments involving two pulsed beams and several molecular levels. In this section several such situations are briefly discussed.

The most closely related experiment is delayed CSRS of the excited state as depicted in Fig. 1(b). The resonance corresponding to the coherence between $|c\rangle$ and $|d\rangle$ is known to be absent in the $\chi^{(3)}$ formalism unless there is pure dephasing in the system.[4,12,41–43] This prevents the measurement of the transverse relaxation of this coherence by steady-state CSRS at the lowest temperatures, though the experimental situation can be misleading,[10] since there are allowed one-photon $\chi^{(3)}$ resonances. The steady-state CSRS experiment has been demonstrated on excited-state vibrations of pentacene in benzoic acid with the line amplitude thermally induced.[12] The delayed analog of this experiment does not require pure dephasing and thus is applicable at lower temperature. Appendix B contains a brief calculation demonstrating that, in the transient resonant regime, vibrational coherence is as easily prepared in the excited state as in the ground state. The nonperturbative approach to CSRS will be discussed more fully elsewhere.

A somewhat different effective four-level system arises in the case of a dimer of two inequivalent guest molecules. Here four electronic states are formed from the monomer S_0 and S_1 states by the intermolecular interaction. In a recent study of such a pentacene dimer in *p*-terphenyl,[61] the relative energies of these four states were located using low-temperature CSRS resonances. Here a time-domain experiment should prove valuable for measuring the transverse relaxation between the two singly excited dimer states, since within the $\chi^{(3)}$ formalism this quantity would again only be observable once pure dephasing set in. The probe pulse calculation presented in Sec. III can be readily extended to probing the double quantum coherence in dimers as well.

Particularly when electronic states are involved, the possibility arises that an inhomogeneity over the sample of the frequency of the prepared coherence could cause additional dephasing which would obscure the underlying T_2. Such inhomogeneous decay can be eliminated by interchanging the populations of the states involved with an additional pair of simultaneous pulses at ω_1 and ω_2 at $t_1/2$ (Raman echo).[36–40] The formalism here allows the calculation of the efficiency of this process for different pulse parameters. For example, for either of the frequency arrangements on the left sides of Fig. 1(a) or 1(b), the echo efficiency in terms of intensity cannot exceed 25% with $\Delta=0$. This result represents the limit where three levels participate and is already known[48] from previous calculations, which differ from the case of the Raman echo only in the means assumed of detecting the echoed coherence. This situation differs from the 100% echo efficiency (π pulse) possible for the usual two-level echo[62] and the pseudo-two-level model of the Raman echo[36–38]

applicable at large Δ.

The application of two simultaneous intense fields near electronic transitions may also be useful for studies of vibronic coherence. Though the focus in Sec. III B was on the vibrational coherence prepared, the last term of (3.26) describes coherence between the previously unoccupied states $|b\rangle$ and $|c\rangle$. It is prepared by the same pulses. If a π pulse at $\omega_2 \simeq \omega_{cb}$ were to follow after a delay $t_1/2$, then an echo would be formed at ω_{cb} at time t_1, which could be detected, for example, by picosecond gating[52] in potassium dihydrogen phosphate (KDP) with another ω_1 pulse. Such an experiment would complement photon echo studies on vibronic transitions involving the ground state $|a\rangle$,[57,59] which are accessible with single-frequency preparation pulses.

B. Summary

In this work a nonperturbative approach to delayed four wave mixing is developed and applied to the ground-state vibrational CARS spectroscopy of dilute pentacene in molecular crystal hosts. Expressions for the dependence of the signal on the pulse parameters to all orders in the field are derived for short pulses within a four-level model. Connections are drawn to previous results from perturbation theory.

The theoretical expectations for the spectral distribution and the total intensity of the signal as a function of probe pulse energy are compared with experiment, thereby demonstrating the existence of an FID component and effects of large-angle optical nutation. The analysis shows that spatial beam inhomogeneity as well as the length and energy of the probe pulse can limit the sensitivity of the method.

Low-temperature time-domain vibrational T_2 measurements on the $\sim 756\text{-cm}^{-1}$ vibration in a benzoic acid host are found to be inconsistent with previous steady-state measurements.[12] The same time-domain experiment in a naphthalene host necessitates a reinterpretation of previous right angle luminescence experiments.[58]

ACKNOWLEDGMENTS

The investigations were supported by the Netherlands Foundation for Chemical Research (Stichting Scheikundig Onderzoek in Nederland) with financial aid from the Netherlands Organization for the Advancement of Pure Research (Nederlandse Organisatie voor Zuiver-Wetenschappelijk Onderzoek).

APPENDIX A: AVERAGING OVER INHOMOGENEOUS BEAM PROFILES

In the limit that the field at the detector follows in proportion to the sample polarization (3.39) it may be written as

$$\begin{aligned} E_{ab}^{\omega_3}(t') = A \sin(\epsilon_{bd}^{(1')} t'/2)\{&(\cos 2\eta + 1 - \sin 2\eta)\sin[(\omega_3 + n/2 + J/2)t'] \\ &+ (-\cos 2\eta + 1 - \sin 2\eta)\sin[(\omega_3 + n/2 - J/2)t'] \\ &+ (\cos 2\eta + 1 - \sin 2\eta)\sin[(\omega_3 - n/2 + J/2)t'] \\ &+ (-\cos 2\eta + 1 + \sin 2\eta)\sin[(\omega_3 - n/2 - J/2)t']\} \ . \end{aligned} \tag{A1}$$

The factor A represents all the proportionality constants due to preparation, evolution, propagation geometry, and the transition dipole μ_{ad}. The time variable t' includes the propagation delay and has its origin at the moment the first signal reaches the detector. The trigonometric function is just a rearrangement of the real part of the term in bold parentheses in (3.39). Implicit in writing (A1) are the conditions that the time scale for changes in the polarization envelope ($\sim 10^{-12}$ sec) is much longer than an optical period ($\sim 10^{-14}$ sec) and that the envelope of the signal pulse is not reshaped during propagation. The latter condition is consistent with the neglect throughout of any reaction of the system to its own polarization.

At any time t' this quantity must be averaged over the points in the sample at the same $\vec{k}_3 \cdot \vec{r}$, but at different distances R from the beam center. This is the integral

$$\langle E_{ab}^{\omega_3}(t') \rangle = \int_0^\infty E_{ab}^{\omega_3}(t', R) R \, dR \int_0^{2\pi} d\phi \ . \tag{A2}$$

The dependence on R, which is not explicit in (A1), is given by the distribution (4.2) and enters through all of the $\epsilon_{ij}^{(\alpha)}$.

Since the preparation process was chosen to be linear in each of the two beams, the constant A is proportional to the square of the distribution:

$$A(R) = A(0)\exp(-2CR^2) = A(0)u^2(R) \ . \tag{A3}$$

The distribution enters linearly in each of the Rabi frequencies appearing in the probe process. These are proportional to one another,

$$\epsilon_{ac}^{(1')}(R)=K\epsilon_{bd}^{(1')}(R)\ , \tag{A4}$$

but the constant K is unknown. For purposes of calculation $K=1$ will be assumed, since both transitions are ones in which to the lowest approximation the vibrational state does not change. Thus the Franck-Condon factors are expected to be similar. In any case, the calculation will turn out to be quite insensitive to $\epsilon_{ac}^{(1')}$ and thus to K, because it enters the probing only through a nonresonant process. The dependence on $\epsilon_{ac}^{(1')}$ is through the quantities η and n and is given by (3.30b) and (3.32b), respectively.

The contributions from the second and third terms of (A1) may be dropped in evaluating the signal energy. These correspond for $J<0$ to the outermost four lines in Fig. 4. These contributions are small and of opposite phase so they are easily washed out by a distribution in ϵ_{bd}'. Thus it is not surprising that they were not observed in the experiment of Fig. 7. More importantly, for simulation of the total intensity measurements of Fig. 8 they are rigorously absent, because they fall outside of the bandpass of the double monochromator when it is centered at ω_3 and thus make no contribution to the observations.

The next step is to rearrange the contributing terms of (A1) in order to factor out the high-frequency time dependence at ω_3 from the slower modulation of the amplitude envelope. This gives

$$\begin{aligned}E_{ab}^{\omega_3}(R,t')\simeq & A(R)\sin[\epsilon_{bd}^{(1')}(R)t'/2]\\ &\times(2\sin(\omega_3 t')\cos\{[n(R)+J]t'/2\}+\cos(\omega_3 t')\{\cos[2\eta(R)]+\sin[2\eta(R)]\}\\ &\times\sin\{[n(R)+J]t'/2\})\ .\end{aligned} \tag{A5}$$

Substituting (A5) into (A2) and using (A3), the desired fluence integral representing the signal contribution from scattering during the probe pulse may be written as

$$\Phi_{\text{pulse}}=\int_0^{\tau'} I_{ab}^{\omega_3}(t')dt' \tag{A6a}$$

$$=\int_0^{\tau'}\langle E_{ab}^{\omega_3}(t')\rangle^2 dt' \tag{A6b}$$

$$\begin{aligned}=A^2(0)\int_0^{\tau'}(&2\langle u^2(R)\sin[\epsilon_{bd}^{(1')}(R)t'/2]\cos[(n(R)+J)t'/2]\rangle^2\\ &+\tfrac{1}{2}\langle u^2(r)\sin[\epsilon_{bd}^{(1')}(R)t'/2]\{\cos[2\eta(R)]+\sin[2\eta(R)]\}\sin\{[n(R)+J]t'/2\}\rangle^2)dt'\ .\end{aligned} \tag{A6c}$$

In writing the integrand in (A6c), an averaging over an optical period has already been carried out using the fact that ω_3 is much faster than any of the other frequencies. Thus this integrand is the envelope of the intensity. The spatial integrals, which are indicated by the brackets, are of the form of (A2).

APPENDIX B: EXCITED-STATE CSRS

The excited-state CSRS resonance in $\chi^{(3)}$ at $(\omega_2-\omega_1)=\omega_{dc}$ is known to vanish in the absence of any pure dephasing among the levels involved.[4,12,41–43] This interesting phenomenon is peculiar to the steady-state response at low field intensity. The delayed CSRS experiment near electronic resonance is capable of measuring the transverse vibrational decay in the absence of pure dephasing and thus to arbitrarily low temperature. Furthermore, this transient response appears to third order in the fields and so does not have a qualitatively different requirement on pulse power near resonance than does ground-state delayed CARS.

To see this we calculate the preparation dynamics for the fully resonant case corresponding to $\Delta=0$ on the left-hand side of Fig. 2(b). In analogy to (3.16) the Hamiltonian is

$$\mathcal{H}_3^{(0)}=\epsilon(\cos\theta\, I_x^{ac}+\sin\theta\, I_x^{ad})\ , \tag{B1}$$

where now

$$\theta=\tan^{-1}(\epsilon_{ad}^{(2)}/\epsilon_{ac}^{(1)}) \tag{B2}$$

and

$$\epsilon=[(\epsilon_{ac}^{(1)})^2+(\epsilon_{ad}^{(2)})^2]^{1/2}\ . \tag{B3}$$

The analog of (3.26) [also with $\rho(0)=|a\rangle\langle a|$] is then found to be

$$U_3(\tau)\rho(0)U_3(\tau)$$
$$=\tfrac{1}{3}(|a\rangle\langle a|+|c\rangle\langle c|+|d\rangle\langle d|)+\tfrac{1}{6}[1+3\cos(\epsilon\tau)](I_z^{ad}+I_z^{ac})-\tfrac{1}{2}[1-\cos(\epsilon\tau)]\cos(2\theta)I_z^{cd}$$
$$+\tfrac{1}{2}[1-\cos(\epsilon\tau)]\sin(2\theta)I_x^{cd}-\sin(\epsilon\tau)\cos\theta\, I_y^{ad}-\sin(\epsilon\tau)\sin\theta\, I_y^{ac}\ . \tag{B4}$$

The coefficient desired is

$$\rho_{dc}(\tau)=\tfrac{1}{4}[1-\cos(\epsilon\tau)\sin(2\theta)]\ . \tag{B5}$$

Comparing this to (3.27), it is clear that the preparation of coherence between two originally unoccupied states $|c\rangle$ and $|d\rangle$ has somewhat simpler dynamics. There is no Fourier component at $\epsilon/2$. However, expanding (B5) to order $(\epsilon\tau)^2$ gives

$$\rho_{dc}(\tau)=(\epsilon\tau)^2\sin(2\theta)/4 \tag{B6a}$$
$$=(\tau^2/2)\epsilon_{ad}^{(2)}\epsilon_{ac}^{(1)}\ , \tag{B6b}$$

so just as in (3.28), the vibrational coherence appears to second order in the applied fields. The probe pulse calculation is isomorphic to that for ground-state CARS and shows a signal at $\omega_2\simeq\omega_{cb}$ to first order in the probe pulse. Thus the overall process is third order. There is no contradiction with the conclusion that this process is forbidden in $\chi^{(3)}$, since the calculation here only shows that a transient, not a steady-state response is possible to third order. This is entirely adequate for the delayed experiment.

[1]N. Bloembergen, *Nonlinear Optics* (Benjamin, New York, 1965).

[2]P. D. Maker and R. W. Terhune, Phys. Rev. 137, A801 (1965).

[3]C. Flytzanis, in *Quantum Electronics,* edited by H. Rabin and C. L. Tang (Academic, New York, 1975), Vol. 1, Part A, Ch. 2.

[4]N. Bloembergen, H. Lotem, and R. T. Lynch, Indian J. Pure Appl. Phys. 16, 151 (1978).

[5]S. A. J. Druet, B. Attal, T. K. Gustafson, and J. P. Taran, Phys. Rev. A 18, 1529 (1978).

[6]S. Y. Yee and T. K. Gustafson, Phys. Rev. A 18, 1597 (1978).

[7]J. L. Oudar and Y. R. Shen, Phys. Rev. A 22, 1141 (1980).

[8]B. S. Hudson, W. H. Hetherington, S. P. Cramer, I. Chabay, and G. K. Klauminzer, Proc. Nat'l. Acad. Sci. (U.S.A.) 73, 3798 (1976).

[9]L. A. Carreira, T. C. Maguire, and T. B. Malloy, Jr., J. Chem. Phys. 66, 2621 (1977).

[10]P. L. Decola, J. R. Andrews, R. M. Hochstrasser, and H. P. Trommsdorff, J. Chem. Phys. 73, 4695 (1980).

[11]J. R. Andrews, R. M. Hochstrasser, and H. P. Trommsdorff, Chem. Phys. 62, 87 (1981).

[12]J. R. Andrews and R. M. Hochstrasser, Chem. Phys. Lett. 82, 381 (1981).

[13]J. R. Andrews and R. M. Hochstrasser, Chem. Phys. Lett. 83, 427 (1981).

[14]R. R. Alfano and S. L. Shapiro, Phys. Rev. Lett. 26, 1247 (1971).

[15]D. von der Linde, A. Laubereau, and W. Kaiser, Phys. Rev. Lett. 26, 954 (1971).

[16]A. Laubereau and W. Kaiser, Rev. Mod. Phys. 50, 607 (1978).

[17]I. Abram, R. M. Hochstrasser, J. E. Kohl, M. G. Semack, and D. White, Chem. Phys. Lett. 52, 1 (1977); J. Chem. Phys. 71, 153 (1979).

[18]C. H. Lee and D. Ricard, Appl. Phys. Lett. 32, 168 (1978).

[19]W. Zinth, A. Laubereau, and W. Kaiser, Opt. Commun. 26, 457 (1978).

[20]J. P. Heritage, Appl. Phys. Lett. 34, 470 (1979).

[21]F. M. Kamga and M. G. Sceats, Opt. Lett. 5, 126 (1980).

[22]I. C. Khoo and R. F. Code, Opt. Commun. 32, 145 (1980).

[23]T. J. Aartsma, W. H. Hesselink, and D. A. Wiersma, Chem. Phys. Lett. 71, 424 (1980).

[24]B. H. Hesp and D. A. Wiersma, Chem. Phys. Lett. 75, 423 (1980).

[25]K. Duppen, B. H. Hesp, and D. A. Wiersma, Chem. Phys. Lett. 79, 399 (1981).

[26]F. Ho, W.-S. Tsay, J. Trout, and R. M. Hochstrasser, Chem. Phys. Lett. 83, 5 (1981).

[27]W. Zinth, H.-J. Polland, A. Laubereau, and W. Kaiser, Appl. Phys. B26, 77 (1981).

[28]P. Ye and Y. R. Shen, Phys. Rev. A 25, 2183 (1982).

[29]J. Kuhl, Appl. Phys. B28, 251 (1982).

[30]K. Duppen, D. P. Weitekamp, and D. A. Wiersma, in *Picosecond Phenomena, III,* edited by A. Laubereau and K. B. Eisenthal (Springer, Berlin, 1982).

[31](a) D. P. Weitekamp, K. Duppen, and D. A. Wiersma, Appl. Phys. B29, 178 (1982); (b) K. Duppen, D. P. Weitekamp, and D. A. Wiersma (unpublished).

[32]M. D. Duncan, P. Oesterlin, F. Konig, and R. L. Byer, Chem. Phys. Lett. 80, 253 (1981).

[33]A. D. Wilson-Gordon, R. Klimovsky-Barid, and H. Friedmann, Phys. Rev. A 25, 1580 (1982).

[34]F. A. M. de Oliveira, C. B. de Araújo, and J. R. Rios Leite, Phys. Rev. A 25, 2430 (1982).

[35]A. D. Wilson-Gordon and H. Friedmann, Chem. Phys. Lett. 89, 273 (1982).

[36]S. R. Hartmann, IEEE J. Quantum Electron. QE-4, 802 (1968).
[37]P. Hu, S. Geschwind, and T. M. Jedju, Phys. Rev. Lett. 37, 1357 (1976).
[38]P. Hu, S. Geschwind, and T. M. Jedju, in *Coherence and Quantum Optics, IV,* edited by L. Mandel and E. Wolf (Plenum, New York, 1978).
[39]K. P. Leung, T. W. Mossberg, and S. R. Hartmann, Phys. Rev. A 25, 3097 (1982).
[40]J. Langelaar, D. Bebelaar, and J. D. W. van Voorst, Appl. Phys. B28, 274 (1982).
[41]Y. Prior, A. R. Bogdan, M. Dagenais, and N. Bloembergen, Phys. Rev. Lett. 46, 111 (1981).
[42]A. Bogdan, M. Downer, and N. Bloembergen, Phys. Rev. A 24, 623 (1981).
[43]N. Bloembergen, A. R. Bogdan, and M. W. Downer, in *Laser Spectroscopy V,* edited by A. R. W. McKellar, T. Oka, and B. P. Stoicheff (Springer, Berlin, 1981), p. 158.
[44]A. Wokaun and R. R. Ernst, J. Chem. Phys. 67, 1752 (1977).
[45]S. Vega, J. Chem. Phys. 68, 5518 (1978).
[46]U. Haeberlen and J. S. Waugh, Phys. Rev. 175, 453 (1968).
[47]F. Bloch and A. Siegert, Phys. Rev. 57, 522 (1940).
[48]M. Aihara and H. Inaba, Opt. Commun. 8, 280 (1973); J. Phys. A 6, 1709 (1973).
[49]M. Mehring, E. K. Wolff, and M. E. Stoll, J. Magn. Reson. 37, 475 (1980).
[50]H. Hatanaka and T. Hashi, Phys. Rev. B 21, 2677 (1980).
[51]F. T. Hioe and J. H. Eberly, Phys. Rev. A 25, 2168 (1982).
[52]W. H. Hesselink and D. A. Wiersma, Chem. Phys. Lett. 56, 227 (1978).
[53]C. K. Chan and S. O. Sari, Appl. Phys. Lett. 25, 403 (1974).
[54]C. V. Shank and E. P. Ippen, Appl. Phys. Lett. 24, 373 (1974).
[55]H. P. Weber and H. G. Danielmeyer, Phys. Rev. A 2, 2074 (1970).
[56]H. Mahr and M. D. Hirsch, Opt. Commun. 13, 96 (1975).
[57]W. H. Hesselink and D. A. Wiersma, J. Chem. Phys. 73, 648 (1980).
[58]P. de Bree and D. A. Wiersma, Chem. Phys. Lett. 88, 17 (1982).
[59]W. H. Hesselink and D. A. Wiersma, J. Chem. Phys. 74, 886 (1981).
[60]P. de Bree and D. A. Wiersma, J. Chem. Phys. 70, 790 (1979).
[61]H. B. Levinsky and D. A. Wiersma, Chem. Phys. Lett. 92, 24 (1982).
[62]E. L. Hahn, Phys. Rev. 80, 580 (1950).